



Arginase 1 and L-arginine coordinate fetal lung development and the initiation of labor in mice

Yaqin Yu^{1,†}, Yuanyuan Liu^{1,†} , Xuesong Sui^{1,†}, Yanyu Sui¹, Zhe Wang¹, Carole R Mendelson^{2,3} & Lu Gao^{1,4,*} 

Abstract

Fetal development and parturition are precisely regulated processes that involve continuous crosstalk between the mother and the fetus. Our previous discovery that wild-type mice carrying steroid receptor coactivator (Src)-1 and Src-2 double-deficient fetuses exhibit impaired lung development and delayed labor, which indicates that the signals for parturition emanate from the fetus. In this study, we perform RNA sequencing and targeted metabolomics analyses of the lungs from fetal *Src-1/-2* double-knockout mice and find that expression of arginase 1 (*Arg1*) is significantly decreased, accompanied by increased levels of the *Arg1* substrate L-arginine. Knockdown of *Arg1* in the lungs of fetal mice induces apoptosis of epithelial cells and dramatically delays initiation of labor. Moreover, treatment of human myometrial smooth muscle cells with L-arginine significantly inhibits spontaneous contractions by attenuating activation of NF- κ B and downregulating expression of contraction-associated protein genes. Transcription factors GR and C/EBP β increase transcription of *Arg1* in an Src-1/Src-2-dependent manner. These findings provide new evidence that fetus-derived factors may play dual roles in coordinating fetal lung development and the initiation of labor.

Keywords arginase 1; arginine; fetal lung development; parturition; steroid receptor coactivators

Subject Categories Chromatin, Transcription, & Genomics; Development; Metabolism

DOI 10.15252/embr.202256352 | Received 22 October 2022 | Revised 18 May 2023 | Accepted 24 May 2023 | Published online 9 June 2023

EMBO Reports (2023) 24: e56352

Introduction

Preterm birth (childbirth prior to 37 weeks of gestation), the leading cause of mortality and morbidity in newborns and children under 5 years of age (Liu *et al.*, 2016), accounts for approximately 33% of neonatal deaths (Song *et al.*, 2016; da Fonseca *et al.*, 2020). Babies that survive the immediate consequences of their preterm birth manifest a

significant increase in the incidence of a number of adverse conditions, including long-term neurodevelopmental disorders, impaired lung alveolar development with bronchopulmonary dysplasia, and compromised vision and hearing, which cause emotional and financial burdens to families and adversely impact the public healthcare systems (Fuchs & Senat, 2016; Koullali *et al.*, 2016; Glover & Manuck, 2018). Unfortunately, over the past several decades, the global incidence of preterm birth has not improved (Liu *et al.*, 2016).

In fact, both preterm and post-term delivery represent abnormalities in the molecular mechanisms underlying the initiation of labor. To effectively prevent these parturition disorders, it is necessary to define the complex mechanisms that involve interactive communications between the mother and fetus (Condon *et al.*, 2004; Mendelson, 2009; Romero *et al.*, 2014; Gao *et al.*, 2015). However, more studies have focused on the contributions of maternal factors to the initiation of labor (Simmons *et al.*, 2010; Norman & Shennan, 2013), and the concept that fetal organ development and maternal adaptation are coordinated has emerged in recent years (Petraglia *et al.*, 2010; Mendelson *et al.*, 2017).

Since the development and maturation of the fetal lungs and secretion of pulmonary surfactant are critical for air breathing after birth, we considered that surfactant components may serve as potential factors in the timing of parturition. We and others observed that lung surfactant components, SP-A, and the inflammatory glycerophospholipid, platelet-activating factor (PAF), secreted by the fetal lungs into amniotic fluid (AF) during late gestation, serve as hormonal signals for the initiation of parturition (Frenkel *et al.*, 1996; Condon *et al.*, 2004; Gao *et al.*, 2015). We found that WT pregnant mice carrying fetuses that were double deficient in steroid receptor coactivators (Src)-1 and Src-2 (*Src-1/-2^{d/d}*) manifested a delay in parturition by 1 ~ 2 days, caused by a deficiency in SP-A and PAF production by the fetal lungs and secretion into amniotic fluid (Gao *et al.*, 2015).

SRCs do not directly bind to the promoter regions of genes but can significantly increase nuclear receptor-mediated gene transcription by interacting with nuclear receptors bound to these regions, recruiting histone acetylases, which increase histone acetylation to open chromatin and increase gene transcription (Lonard & O'Malley, 2007). *Src-1/-2* double-knockout (dKO) mice die at birth of respiratory distress (Mark *et al.*, 2004) because of impaired lung development (Chen

1 Department of Physiology, Naval Medical University, Shanghai, China

2 Department of Biochemistry, University of Texas Southwestern Medical Center, Dallas, TX, USA

3 Department of Obstetrics and Gynecology, University of Texas Southwestern Medical Center, Dallas, TX, USA

4 Shanghai Key Laboratory for Assisted Reproduction and Reproductive Genetics, Shanghai, China

*Corresponding author. Tel: +86 21 81870980; E-mail: roadgao@163.com

[†]These authors contributed equally to this work

et al, 2020) and decreased production of the major surface tension lowering component of lung surfactant, dipalmitoylphosphatidylcholine (DPPC) (Gao et al, 2015). Recently, we observed that the lungs of *Src-1/-2* dKO fetal mice have significantly reduced expression of 11 β -hydroxysteroid dehydrogenase 1 (11 β -HSD1), which contributes to decreased glucocorticoid responsiveness (Chen et al, 2020). To identify other fetal lung-derived factors that contribute to fetal lung development and the initiation of parturition, in this study, we further explored alterations in gene expression in the lungs of *Src-1/-2* dKO fetal mice, compared to WT. Intriguingly, we observed that expression of two genes involved in arginine metabolism and biosynthesis, arginase 1 (*Arg1*) and argininosuccinate synthase 1 (*Ass1*), was significantly altered in lungs of *Src-1/-2* dKO mice, compared to WT.

Results

RNA sequencing of fetal lungs from WT and *Src-1* and/or *Src-2*-KO mice at 18.5 dpc

To identify alterations in gene expression in fetal lungs of *Src-1* KO and/or *Src-2* KO mice, we performed RNA-seq analysis on lungs

from WT, *Src-1* KO, *Src-2* KO, and *Src-1/-2* dKO fetuses at 18.5 days post-coitum (dpc). A total of 61, 32, 11, 901, and 480 significant DEGs were identified in the *Src-1*KO versus WT, *Src-2*KO versus WT, *Src-1/-2* dKO versus *Src-1*KO, *Src-1/-2* dKO versus *Src-2*KO, and *Src-1/-2* dKO versus WT comparisons, respectively (Dataset EV1; Fig 1A). Since delayed labor only occurred when the fetuses were deficient in both *Src-1* and *Src-2*, we focused on the 480 DEGs in the fetal lungs of *Src-1/-2* dKO versus WT mice. The top 10 biological process pathways that were significantly different in *Src-1/-2* dKO versus WT according to gene ontology (GO) analysis are listed (Fig 1B). Among these pathways, several were shown to be closely related to organ development. Since *Src-1/-2* dKO mice displayed abnormal lung development (Chen et al, 2020), it was of interest that nine DEGs, including *Crh*, *Gli3*, *Mycn*, *Gli1*, *Arg1*, *Lif*, *Crispld2*, *Ccbe1*, and *Hsd11b1*, were found to be associated with the lung development pathway (Fig 1C). One of the transcripts that was markedly downregulated in the lungs of *Src-1/-2* dKO mice compared to WT was *Arg1*, which encodes a key enzyme that catalyzes the metabolism of arginine to ornithine and urea. Therefore, we looked over the DEGs involved in the amino acid biosynthesis and metabolism pathways using the Kyoto Encyclopedia of Genes and Genomes (KEGG) analysis and found that another gene termed *Ass1*

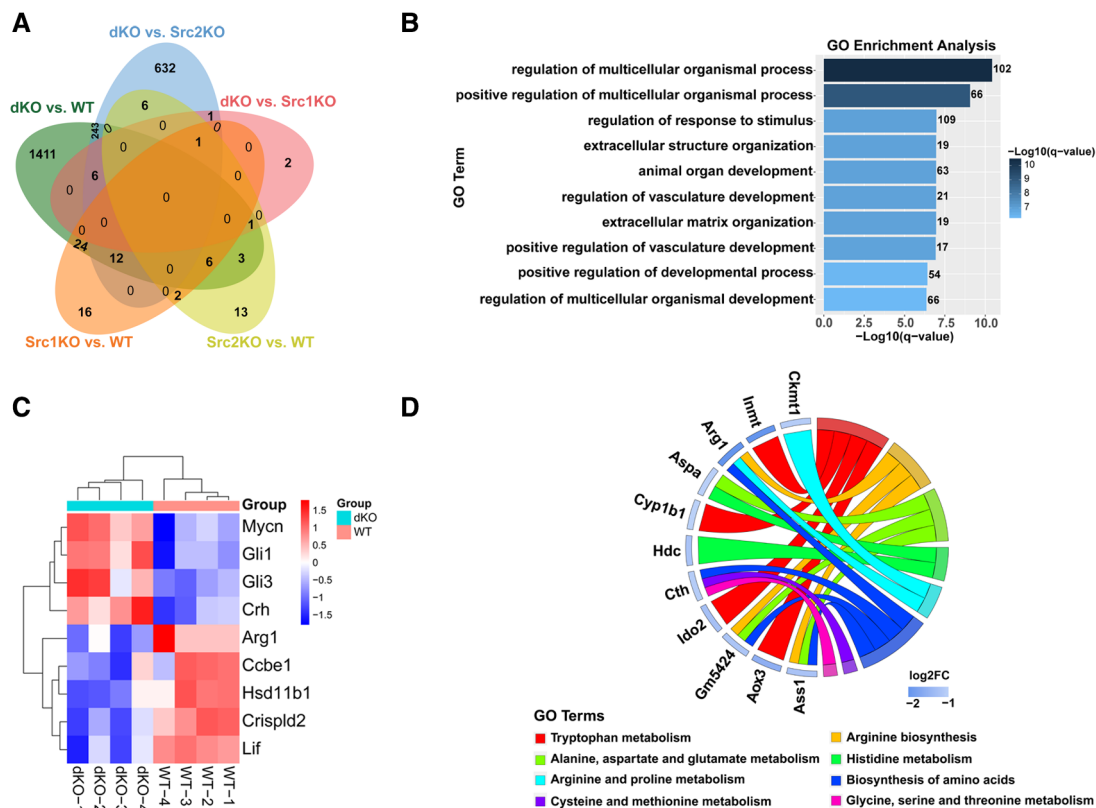


Figure 1. RNA expression profile and GO analysis of the lungs from WT, *Src-1* KO, *Src-2* KO, and *Src-1/-2* dKO fetuses at 18.5 dpc.

- A Venn diagram showing the number of DEGs in each group.
 B Horizontal bar chart demonstrates the top 10 GO terms of biological processes in which the DEGs between *Src-1/-2* dKO versus WT groups are enriched. The numbers of DEGs involved in each biological process were listed alongside the corresponding bar.
 C Heatmap of DEGs between the *Src-1/-2* dKO and WT fetuses that are involved in the lung development pathway (GO: 0030324).
 D The DEGs of the lungs between *Src-1/-2* dKO and WT fetuses involved in the amino acid biosynthesis and metabolism pathways using the KEGG analysis.

Source data are available online for this figure.

(argininosuccinate synthetase 1), which is annotated to the arginine biosynthesis pathway along with *Arg1*, was also significantly down-regulated in lungs of *Src-1/-2* dKO mice compared to WT (Fig 1D).

Arg1 and Ass1 expression is significantly decreased in the lungs of *Src-1/-2*dKO fetal mice

Next, we validated the RNA-seq findings by analyzing *Arg1* and *Ass1* mRNA and protein expression in the lungs of WT fetal mice versus lungs of *Src-1* KO, *Src-2* KO, and *Src-1/-2* dKO fetal mice using RT-qPCR and western blotting, respectively (Fig 2A–D). Notably, *Arg1* mRNA levels in the lungs of *Src-1* KO, *Src-2* KO, and *Src-1/-2* dKO fetuses were significantly decreased compared with those of WT fetuses (Fig 2A). ARG1 protein levels in the lungs of *Src-1* KO and *Src-2* KO fetuses also showed decreased trend compared with those of WT fetuses, whereas only the lungs of *Src-1/-2* dKO fetuses exhibited a significant decrease in ARG1 protein levels compared to WT (Fig 2B). In the case of *Ass1*, mRNA levels were significantly decreased in *Src-1/-2* dKO fetal lungs, compared to WT, *Src-1* KO, or *Src-2* KO fetal lungs; however, *Ass1* mRNA levels were not significantly altered in the *Src-1* KO or *Src-2* KO fetal lungs compared to WT (Fig 2C). ASS1 protein levels were also significantly decreased in *Src-1/-2* dKO fetal lungs compared to WT; although ASS1 protein expression showed decreased trend in *Src-2* KO fetal lungs compared to WT, the difference did not reach statistically significant level (Fig 2D). Immunohistochemical (IHC) analysis also showed that protein expression of ARG1 and ASS1 in fetal lungs at 18.5 dpc was decreased in *Src-1/-2* dKO fetuses compared to WT fetuses (Fig 2E and F).

Dynamic temporal changes in Arg1 and Ass1 expression in fetal lungs of WT mice during late gestation

The mRNA levels of *Arg1* were significantly increased in the lungs of WT fetuses at labor, compared to 15.5 and 17.5 dpc. ARG1 protein levels were significantly increased only between labor and 15.5 dpc (Fig 3A and B). *Ass1* mRNA and protein expression also was significantly increased in the lungs of WT fetuses at labor, compared to 15.5 dpc (Fig 3C and D). Additionally, IHC staining showed dynamic increases in ARG1 and ASS1 abundance in the fetal lungs of WT mice from 15.5 dpc to labor (Fig 3E and F). By immunofluorescent staining, ARG1 was found to be dispersedly distributed in cytoplasm of type II alveolar epithelial cells indicated by their marker, lysophosphatidylcholine acyltransferase 1 (LPCAT1) (Fig EV1A), while ASS1 was expressed as aggregates mainly in the cytoplasm of type I alveolar epithelial cells, indicated by their marker, podoplanin (PDPN) (Fig EV1B).

Arg1 and Ass1 metabolites in fetal lungs from *Src-1/-2* dKO mice

ARG1 and ASS1 are key enzymes in the urea cycle and are involved in the metabolism of a number of amino acids. Arg1 hydrolyzes arginine to ornithine and urea, while ASS1 catalyzes conversion of citrulline to arginine succinate (Fig 4A). To assess the levels of ARG1 and ASS1 metabolites in fetal lungs from *Src-1/-2* dKO versus WT mice, liquid chromatography–mass spectrometry (LC–MS) combined with multiple reaction monitoring (MRM) technology was used to analyze nucleotides, amino acids, energy metabolism

intermediates, neurotransmitters, and vitamins in central carbon metabolic pathways (Cai & Zhu, 2019). The principal component analysis (PCA) chart showed that the experimental data were stable and reliable, indicating that the differences in the metabolic profile obtained in the experiment reflect the biological differences between the samples (Fig EV2A). Fifty metabolites were significantly different between the fetal lungs from *Src-1/-2* dKO mice and WT mice (Fig 4B), and both arginine biosynthesis and metabolism pathways were significantly altered according to KEGG pathway analysis (Fig 4C).

The concentration of arginine in the *Src-1/-2* dKO fetal lungs was significantly higher than that of WT fetal lungs, while the concentration of ornithine was significantly reduced in the *Src-1/-2* dKO fetal lungs compared to WT (Fig 4D). These results are consistent with the decreased expression of Arg1 in the *Src-1/-2* dKO fetal lungs. In addition, arginine can also be metabolized by nitric oxide synthase (NOS) to synthesize nitric oxide (NO) (Fig 4A). Although the expression of NOS was not altered in the fetal lungs of *Src-1/-2* dKO mice (Dataset EV1), the levels of asymmetric dimethylarginine (ADMA), an inhibitor of NOS, were significantly increased. Moreover, the ratio of arginine to ADMA was reduced in the lungs of the *Src-1/-2* dKO fetuses compared to WT (Fig 4E), suggesting that the bioavailability of NO was inhibited in *Src-1/-2* dKO fetal lungs.

However, the expression level of ASS1 was also decreased in the fetal lungs of *Src-1/-2* dKO mice, and the concentration of its substrate citrulline was not significantly changed in the lungs of *Src-1/-2* dKO fetal mice compared to WT (Fig EV2B). The level of arginine succinate, the metabolite formed by the action of ASS1, was too low to be detected in the fetal lungs from either WT or *Src-1/-2* dKO mice. Therefore, we focused on the effects of ARG1 and its metabolites on fetal lung development and the initiation of labor.

Knockdown of Arg1 in fetal lungs induces apoptosis of alveolar epithelial cells

To investigate the effects of ARG1 on the development of fetal lungs, adeno-associated virus (pAAV2/9-U6-GFP) carrying either a short hairpin RNA (shRNA) control sequence (AAV-2/9) or *Arg1*-targeting shRNA sequence (AAV-shArg1) was injected into the placenta of each fetus at 13.0 dpc. The pregnant females were euthanized during labor (defined as the delivery of the first pup), and fetal lungs, livers, placenta, and myometrium were harvested for subsequent analyses. GFP expression was evident in the fetal lungs of both AAV-2/9-injected and AAV-shArg1-injected mice (Fig 5A), indicating the high efficiency of AAV infection. The protein abundance of ARG1 was significantly decreased in the fetal lungs of AAV-shArg1-injected mice compared with those of AAV-2/9-injected mice (Fig 5B). Although GFP fluorescence is also highly expressed in fetal liver and maternal myometrium, but not in placenta (Fig EV3A), which is consistent with the GFP mRNA expression pattern in these tissues (Fig EV3B), the expression of ARG1 was not significantly different in fetal livers, placenta, and myometrium between AAV-shArg1-injected mice and AAV-2/9-injected mice (Fig EV3C–E), suggesting the relatively high specificity and efficiency of *Arg1* knockdown in the fetal lungs by AAV-shArg1 injection.

Previous studies have shown that ARG1 is related to proliferation and migration in breast cancer and hepatocellular carcinoma (You et al, 2018; Ming et al, 2020). Therefore, we utilized western

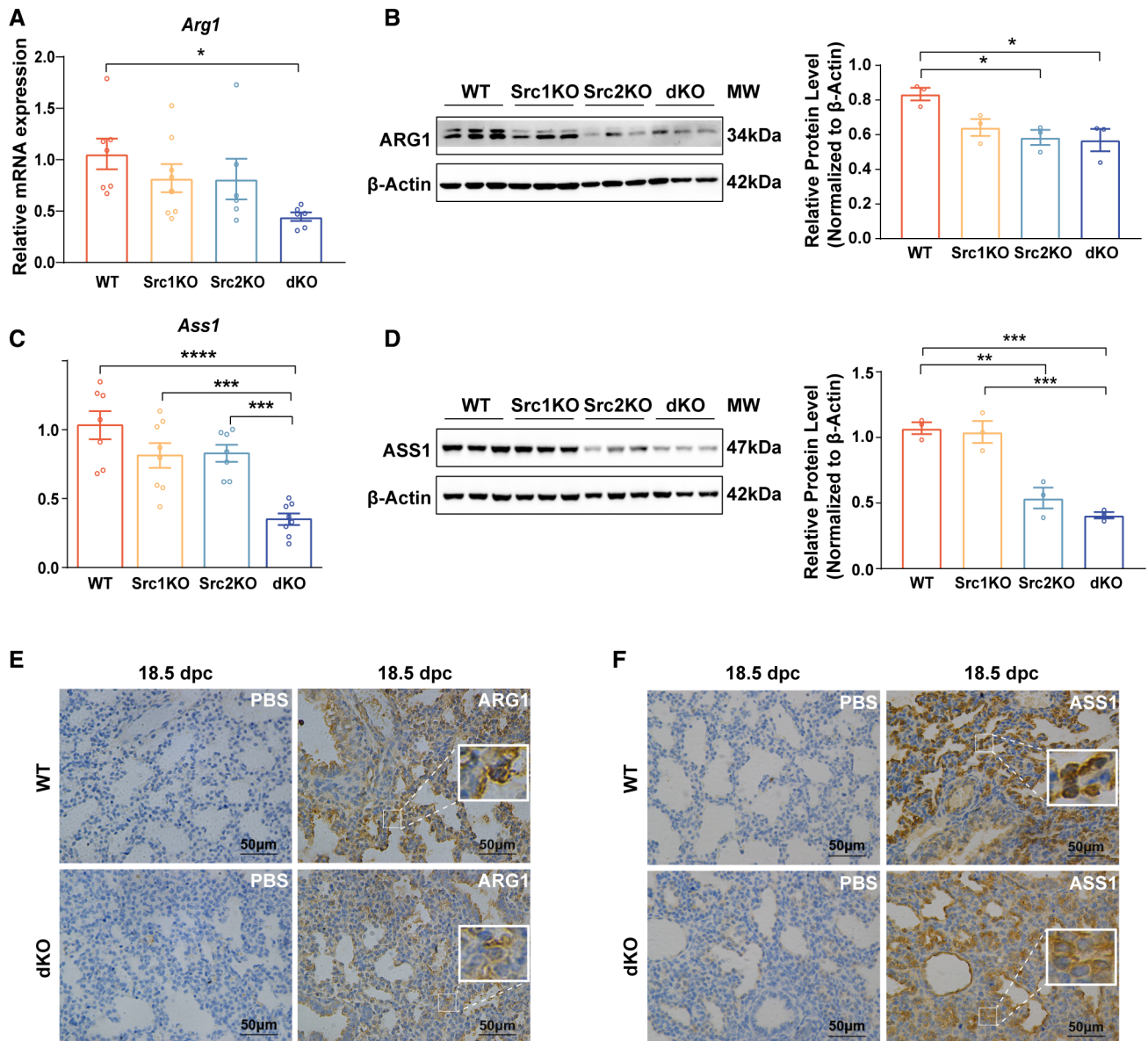


Figure 2. Validation in *Arg1* and *Ass1* mRNA and protein expression in fetal lungs from WT, *Src-1* KO, *Src-2* KO, and *Src-1/2* dKO mice at 18.5 dpc.

A, C mRNA levels of *Arg1* and *Ass1* in fetal lungs of mice with different genotypes at 18.5 dpc; $n = 8$ biological replicates in each group for panel A and seven biological replicates in each group for panel C. One-way ANOVA followed by Tukey's multiple-comparison test was used to analyze the data. The data are shown as the mean \pm s.e.m., * $P < 0.05$, *** $P < 0.001$, and **** $P < 0.0001$, compared with the WT group.

B, D Representative immunoblots of ARG1 and ASS1 protein expression in fetal lungs from mice with different genotypes at 18.5 dpc. Densitometric quantitation of immunoblot scans (relative to β -actin as a loading control) is also shown as a bar graph; $n = 3$ biological replicates in each group. One-way ANOVA followed by Tukey's multiple-comparison test was used to analyze the data. The data are shown as the mean \pm s.e.m., * $P < 0.05$, ** $P < 0.01$, and *** $P < 0.001$, compared with the WT group.

E, F Immunohistochemical staining of ARG1 and ASS1 in fetal lungs of WT and *Src-1/2* dKO mice at 18.5 dpc. PBS was used instead of the primary antibody as a negative control (NC). Scale bars: 50 μ m in (E) and (F).

Source data are available online for this figure.

blotting and immunofluorescence to observe whether the proliferation or apoptosis of fetal lung cells was affected by *Arg1* knock-down. The protein expression of Ki67 was not affected by the knockdown of *Arg1* in fetal lungs (Fig 5C). Consistently, the number of Ki67-positive cells was not different between fetal lungs of AAV-

shArg1-injected mice and those of AAV-2/9-injected mice (Fig 5D). In contrast, although the expression of the inactive caspase3 precursor (pro-caspase3) was comparable in the fetal lung tissues from AAV-shArg1-injected mice and AAV-2/9-injected mice (Fig 5C), the expression of two spliced and active caspase3 proteins (cleaved

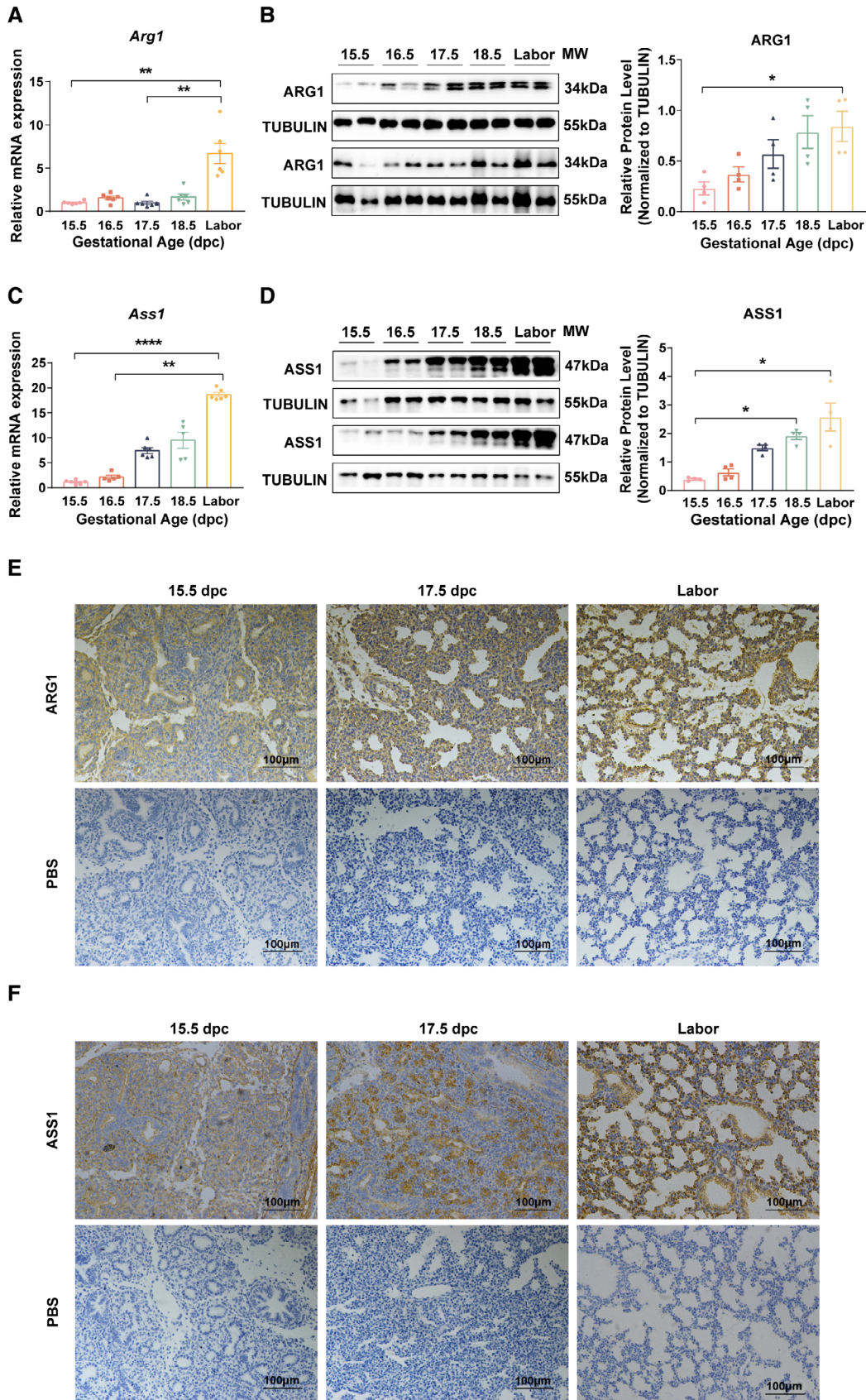


Figure 3.

Figure 3. Dynamic changes in fetal lung *Arg1* and *Ass1* expression in WT mice during late gestation.

- A, C mRNA expression of *Arg1* and *Ass1* in the lungs of WT fetuses at gestational ages from 15.5 dpc to labor. $n = 6$ biological replicates for each gestational age in panel A; $n = 6$ biological replicates for 15.5 dpc, 17.5 dpc, and labor group, $n = 5$ biological replicates for 16.5 and 18.5 dpc group in panel (C). Kruskal–Wallis test followed by Dunn's multiple-comparison test was used to analyze the data. The data shown are the mean \pm s.e.m. $**P < 0.01$ and $****P < 0.0001$.
- B, D Representative immunoblots of gestational changes in ARG1 and ASS1 protein expression in the lungs of WT fetuses at gestational ages from 15.5 dpc to labor. Densitometric quantitation of scans of immunoblots (relative to tubulin as loading control) is also shown as the mean \pm s.e.m. in bar graph; $n = 4$ biological replicates for each gestational age; Kruskal–Wallis test followed by Dunn's multiple-comparison test was used to analyze the data. $*P < 0.05$ compared with 15.5 dpc.
- E, F Immunohistochemical staining of ARG1⁺ (E) or ASS1⁺ (F) cells in the fetal lungs of WT mice at 15.5 dpc, 17.5 dpc, and labor. PBS was used instead of the primary antibody in the NC group. Scale bars: 100 μ m in (E) and (F).
- Source data are available online for this figure.

caspase3) was significantly increased in the fetal lungs of AAV-shArg1-injected mice compared with those of AAV-2/9-injected mice (Fig 5C). Moreover, multiple immunofluorescence stainings showed more TUNEL-positive cells colocalized with either PDPN (type I alveolar epithelial cells marker) staining (Fig 5E) or LPCAT1 (type II alveolar epithelial cells marker) staining (Fig 5F) in the fetal lungs of AAV-shArg1-injected mice than in AAV-2/9-injected mice. To further dissect how the knockdown of *Arg1* induces apoptosis of epithelial cells in fetal lungs, we determined the levels of L-arginine in fetal lungs and found that L-arginine levels significantly increased in fetal lungs after *Arg1* knockdown (Fig EV4A). Then, we treated lung epithelial cell line (A549) with L-arginine at the concentration of 0.1 mg/ml and performed TUNEL staining. It was shown that L-arginine can significantly induce the apoptosis of A549 cells (Fig EV4D). Taken together, these results suggest that the decrease in ARG1 expression has no effect on proliferation but enhances apoptosis of fetal lung cells, especially the alveolar epithelial cells, which may be induced by the aberrant accumulation of L-arginine and affect the development of the fetal lungs.

Arg1 inhibition delays labor due to the attenuation of myometrial cell contractility caused by L-arginine accumulation

Interestingly, we observed that the gestation period of pregnant mice injected with AAV-shArg1 was prolonged and the initiation of labor was delayed. The average gestation period was 21.375 ± 0.473 dpc in mice injected with AAV-shArg1, which was significantly longer than that in mice injected with control AAV (19.5 ± 0.204 dpc) (Fig 6A). It was previously found that L-arginine reduced downstream vascular smooth muscle contractility (Ayers-Ringler et al, 2021), and in the current study, we found that L-arginine levels significantly increased in amniotic fluid although not in myometrium after *Arg1* knockdown (Fig EV4B and C), which suggested that L-arginine might act on the myometrial cells through amniotic fluid in a paracrine manner. We next investigated whether the ARG1 substrate arginine or the Arg1 metabolite ornithine can alter the contractility of the myometrium. hTERT-HSMC cells were embedded in three-dimensional collagen gel matrices and treated with arginine (0.1 mg/ml) or ornithine (0.1 mg/ml) for 24 h. The spontaneous contraction of the gel disk was significantly inhibited by treatment with arginine (Fig 6B), but it was not affected by treatment with ornithine (Figs EV5A and 5B).

To determine the direct cause of delayed labor and attenuated myometrial contractility in AAV-shArg1-injected mice, the expression of contraction-associated proteins (CAPs) in the myometrium

was analyzed. The protein levels of connexin-43 (CX43), oxytocin receptor (OXTR), cyclooxygenase 2 (COX2), and prostaglandin F₂ α receptor (PTGFR) were all significantly decreased in the myometrium of pregnant females injected with AAV-shArg1 compared to that of females injected with control AAV (Fig 6C). Since the genes that encode these contractile proteins are known targets of NF- κ B (32, 33), we further assessed the activation state of NF- κ B. The protein levels of activated NF- κ B, namely its phosphorylated p65 subunit (phospho-S536), were greatly reduced in the myometrial tissues of pregnant females injected with AAV-shArg1 compared to those of females injected with the control AAV (Fig 6D). These findings suggest that the accumulation of arginine due to the knockdown of *Arg1* in fetal lungs may block the activation of NF- κ B in maternal myometrium and inhibit the downstream expression of various CAPs in a paracrine manner; these phenomena may subsequently attenuate the contraction of pregnant uteri near term and eventually lead to delayed labor.

Transactivation of the *Arg1* promoter is enhanced by GR and C/EBP β in an *Src-1/-2*-dependent manner

Many studies have shown that glucocorticoids play an important role in the maturation of fetal lungs (Cole et al, 1995; Bird et al, 2014). In hepatoma cells, it was found that both glucocorticoid receptor (GR) and CCAAT/enhancer-binding protein β (C/EBP β) were required for *Arg1* upregulation induced by glucocorticoids (Gotoh et al, 1997). To investigate the mechanisms underlying *Arg1* transcriptional regulation in fetal lungs, we identified proximal putative glucocorticoid-responsive elements (GREs)- and C/EBP-binding sites in the murine *Arg1* promoter between $-1,000$ and 0 bp relative to the transcription start site (Fig 7A) using the LASAGNA-Search 2.0 online tool (https://biogrid-lasagna.engr.uconn.edu/lasagna_search/) with TRANSFAC matrices.

To assess the recruitment of endogenous GR, SRC-1, SRC-2, and C/EBP β to tethering GRE- and C/EBP-binding sites, ChIP-qPCR was carried out with lung tissues from WT versus *Src-1/-2* dKO fetal mice at 18.5 dpc using qPCR primers flanking each of these sites. Endogenous GR, SRC-1, SRC-2, and C/EBP β were substantially recruited to both GRE- and C/EBP-binding sites in the *Arg1* promoter of the fetal lung tissues of WT mice, whereas the enrichment of GR, SRC-1, SRC-2, and C/EBP β at the GRE- and C/EBP-binding site regions was abolished in *Src-1/-2* dKO mice (Fig 7B–E). As a positive control, the qPCR results of GRE- and C/EBP-binding site for input DNA from WT mouse fetal lung at 18.5 dpc are shown in Fig 7F.

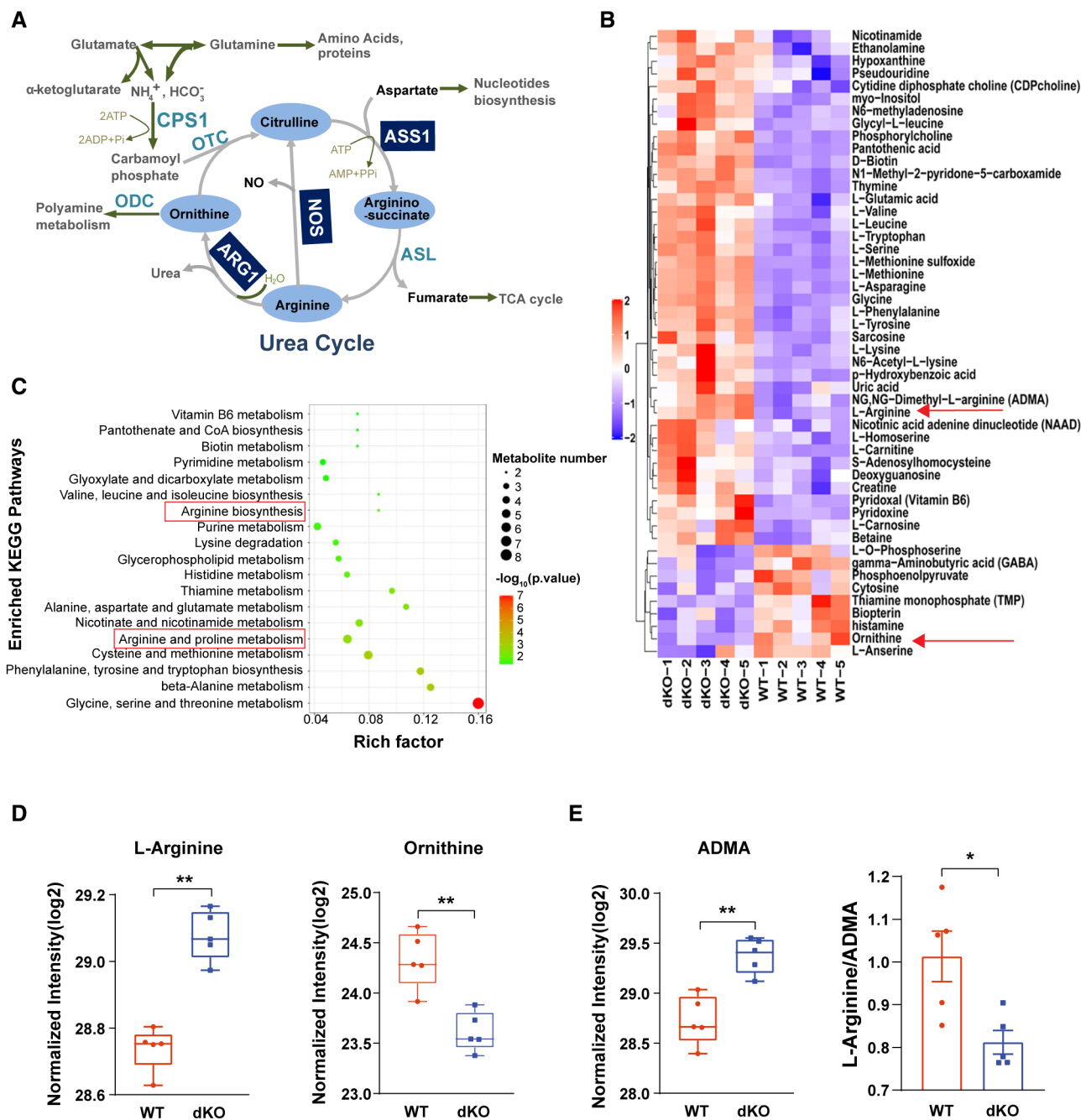


Figure 4. Profile of small-molecule metabolites in the fetal lungs of WT and *Src-1/-2* dKO mice at 18.5 dpc.

A Schematic diagram of the urea cycle.
B Heatmap showing metabolites with significantly different levels in WT versus *Src-1/-2* dKO fetal lungs (P -value < 0.05 and fold change > 1.5). Arginine and ornithine are indicated with red arrows.
C Bubble chart of KEGG pathway enrichment analysis demonstrated that the arginine biosynthesis pathway (highlighted with red box) and arginine and proline metabolic pathways (highlighted with red box) were both significantly enriched.
D, E Histograms showing the content of arginine, ornithine, ADMA, and the ratio of arginine to ADMA in the fetal lungs of WT mice and *Src-1/-2* dKO mice at 18.5 dpc. Mann–Whitney test was used to analyze the data in panel (D), and unpaired t -test was used to analyze the data in panel (E). $n = 5$ biological replicates for each group, and the data are shown as the mean \pm s.e.m. The central band indicates the median, the boxes indicate the upper quartile and lower quartile, and the whiskers indicate maximum value and minimum value of the data. * $P < 0.05$ and ** $P < 0.01$, compared with the WT fetal lungs.

Source data are available online for this figure.

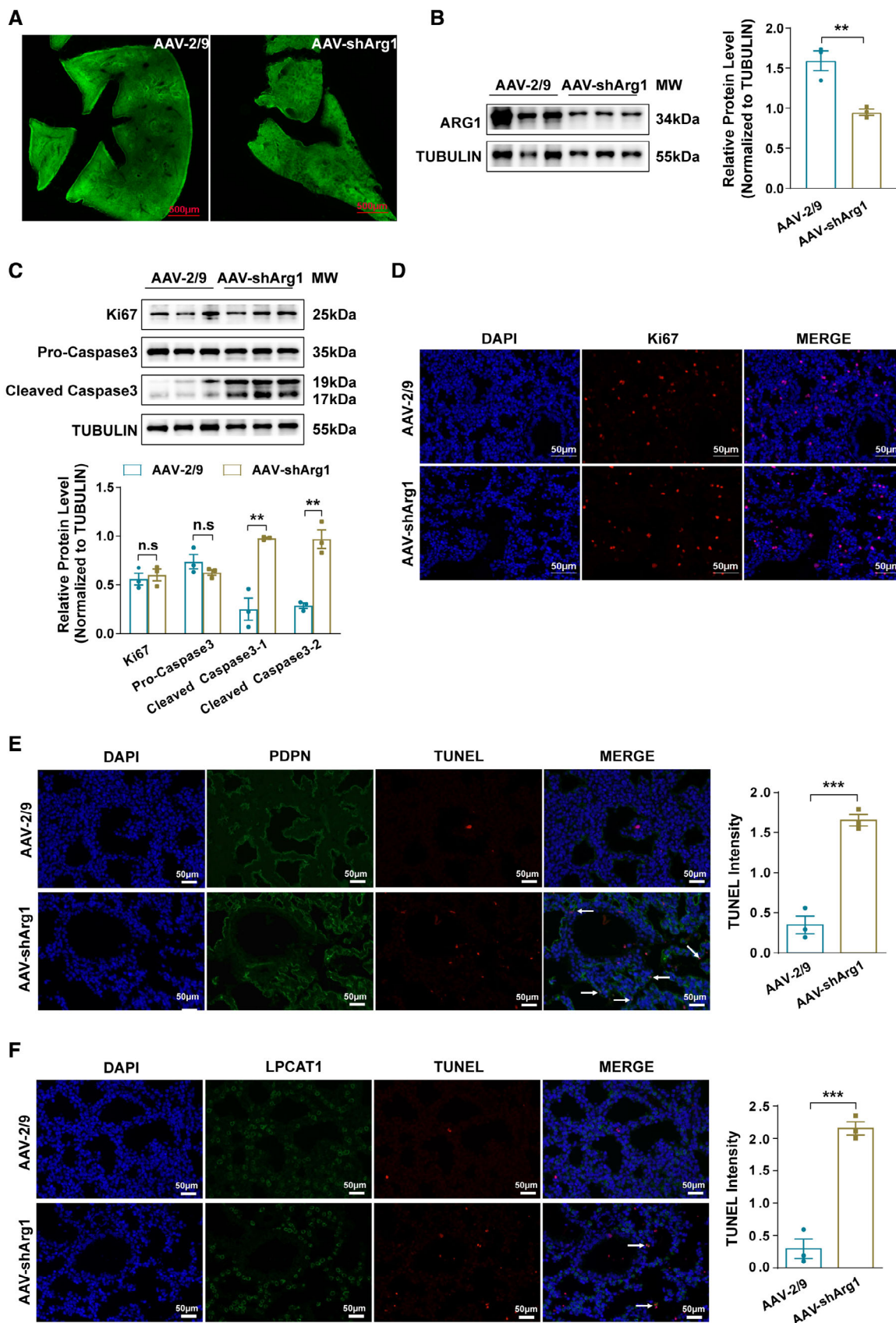


Figure 5.

Figure 5. Knockdown of Arg1 in fetal lungs by placental injection of GFP-tagged, shRNA Arg1-targeting adeno-associated virus (AAV) promotes apoptosis of alveolar epithelial cells.

- A Frozen sections show widespread and intense expression of GFP in the fetal lungs of mice injected with GFP-tagged, Arg1-targeting AAV (AAV-shArg1) or GFP-tagged control AAV (AAV-2/9). Scale bars: 500 μ m.
- B Representative immunoblots of ARG1 expression in the fetal lungs from the AAV-shArg1-injected group and the AAV-2/9-injected group. Densitometric quantitation of scans of immunoblots (normalized to tubulin) is also shown as a bar graph. Unpaired *t*-test was used to analyze the data and *n* = 3 biological replicates for each group. The data are shown as the mean \pm s.e.m. *****P* < 0.01** compared with the AAV-2/9-injected group.
- C Representative immunoblots and densitometric quantitation of Ki67, caspase3 precursor (pro-caspase3), and cleaved caspase3 expression in the fetal lungs from the AAV-shArg1-injected group and AAV-2/9-injected group. Unpaired *t*-test was used to analyze the data and *n* = 3 biological replicates for each group. The data are shown as the mean \pm s.e.m. *****P* < 0.01** compared with the AAV-2/9-injected group; n.s indicates nonsignificant.
- D Immunofluorescence images indicating Ki67+ cells in fetal lung tissues from AAV-shArg1-injected mice or AAV-2/9-injected mice. Blue: DAPI (nuclei); Red: Ki67.
- E Multiple immunofluorescence staining and densitometric quantitation of TUNEL with PDPN antibody (type I alveolar epithelial cells marker) on sections of fetal lungs from AAV-shArg1-injected mice versus AAV-2/9-injected mice. Blue: DAPI (nuclei); Green: PDPN (type I cells); Red: TUNEL positive. Unpaired *t*-test was used to analyze the quantitation data and *n* = 3 biological replicates were generated from the mean intensity of three randomly selected fields of view for each group. The data are shown as the mean \pm s.e.m. ******P* < 0.001** compared with the AAV-2/9-injected group.
- F Multiple immunofluorescence staining and densitometric quantitation of TUNEL with LPCAT1 antibody (type II alveolar epithelial cells marker) on sections of fetal lungs from AAV-shArg1-injected mice versus AAV-2/9-injected mice. Blue: DAPI (nuclei); Green: LPCAT1 (type II cells); Red: TUNEL positive. Unpaired *t*-test was used to analyze the quantitation data and *n* = 3 biological replicates were generated from the mean intensity of three randomly selected fields of view for each group. The data are shown as the mean \pm s.e.m. ******P* < 0.001** compared with the AAV-2/9-injected group.

Data information: Scale bars in (D–F): 50 μ m.

Source data are available online for this figure.

Discussion

During pregnancy, metabolic processes within the mother and fetus undergo substantial changes. Findings from a number of recent studies using nontargeted metabolomic analyses of the peripheral blood from pregnant women indicated that more than half of the metabolites and metabolic pathways change during pregnancy; some of these changes can even be used to accurately predict gestational age and the time of labor (Liang *et al.*, 2020; You *et al.*, 2020). As metabolic sensors and cross-organ coordinators, SRCs regulate food intake, sleep behavior, stress response, and reproduction (Tetel & Acharya, 2013; Stashi *et al.*, 2014; Szwarc *et al.*, 2015), playing important regulatory roles in the metabolism of lipids, carbohydrates, amino acids, and steroids (Stashi *et al.*, 2014). In our previous studies, we found that *Src-1/-2* dKO fetal mice were smaller in overall size, weight, and lung size than WT fetal mice, and their lung maturity was decreased compared to that of WT fetuses (Gao *et al.*, 2015). Further studies also suggested that the signals generated when fetal lungs mature are controlled by *Src-1/Src-2* and are closely associated with the initiation of labor (Gao *et al.*, 2015; Chen *et al.*, 2020). However, the differentially expressed genes and pathways affected by *Src-1/-2* dKO that impair fetal lung development and maturation have not been fully elucidated. In the present study, we used RNA-seq combined with targeted metabolomics to further investigate the changes in the metabolic pathways in the fetal lungs of *Src-1/-2* dKO mice, compared to WT. We found that one of the most highly downregulated genes in fetal lungs of *Src-1/-2* dKO mice was *Arg1*. ARG1 deficiency was associated with a significant increase in arginine levels and a decrease in ornithine levels.

It is of interest that the serotype 9 of AAV we used to package the shArg1 RNA has relative high affinity to fetal lung, fetal liver, and maternal myometrium but very low affinity to placenta, even though the AAV is injected through placenta. Moreover, although AAV-2/9 is incorporated into fetal lung, fetal liver, and myometrium, the mRNA and protein level of Arg1 were significantly knocked down only in fetal lung, but not in fetal liver and myometrium. One of the possible explanations we can propose now is that

the shArg1 RNA sequence might somehow have higher homology with Arg1 DNA in fetal lung than that in other tissues, such as fetal liver and myometrium, so as to manifest higher efficiency of gene knock down in fetal lung, making this serotype of AAV a promising methodology for loss of function or gain of function in the future fetal lung study. Certainly, more studies regarding the fetal lung genomic characteristics need to be done in the future to illustrate if this kind of phenomenon is specific to Arg1 gene or a comprehensive mechanism for a bunch of genes with similar patterns as Arg1.

One of the important functions of ARG1 is to catalyze the hydrolysis of arginine to ornithine and urea in the urea cycle (Sin *et al.*, 2015). L-arginine (L-Arg) is considered to be a “conditionally essential amino acid” in the diet since it is required for survival, growth, and development of conceptuses during the peri-implantation period of pregnancy (Wang *et al.*, 2015). Arginine can also promote placental angiogenesis and growth, improve placental blood flow, and increase the transfer of nutrients from the mother to the fetus (Herring *et al.*, 2018). Arginine at physiological concentrations stimulated maximum ovine trophoblast cell proliferation (Wang *et al.*, 2015). However, in ARG1-deficient patients, a partial or complete loss of the arginase activity affects the urea cycle in the liver, leading to hyperargininemia with spastic paraplegia, progressive neurological and intellectual impairment, persistent growth retardation, and hyperammonemia (Sin *et al.*, 2015; Bjorke-Jenssen *et al.*, 2017; Herring *et al.*, 2018). *Arg1* KO mice are small at birth and differ from wild-type mice in terms of weight and other parameters. They exhibit hyperargininemia, hypoorithinemia, and hyperammonemia and die within 2 weeks (Iyer *et al.*, 2002). In the current study, we found that L-arginine level significantly increased in fetal lung after Arg1 knockdown, and L-arginine can induce lung epithelial cell apoptosis significantly. Consistent with the previous findings, our results once again provide evidence that physiological levels of arginine are critical for normal fetal growth while aberrant accumulation of arginine caused by Arg1 deficiency might impair fetal development.

The development of lung includes five stages, the embryonic stage, the pseudoglandular stage, the canalicular stage, the later

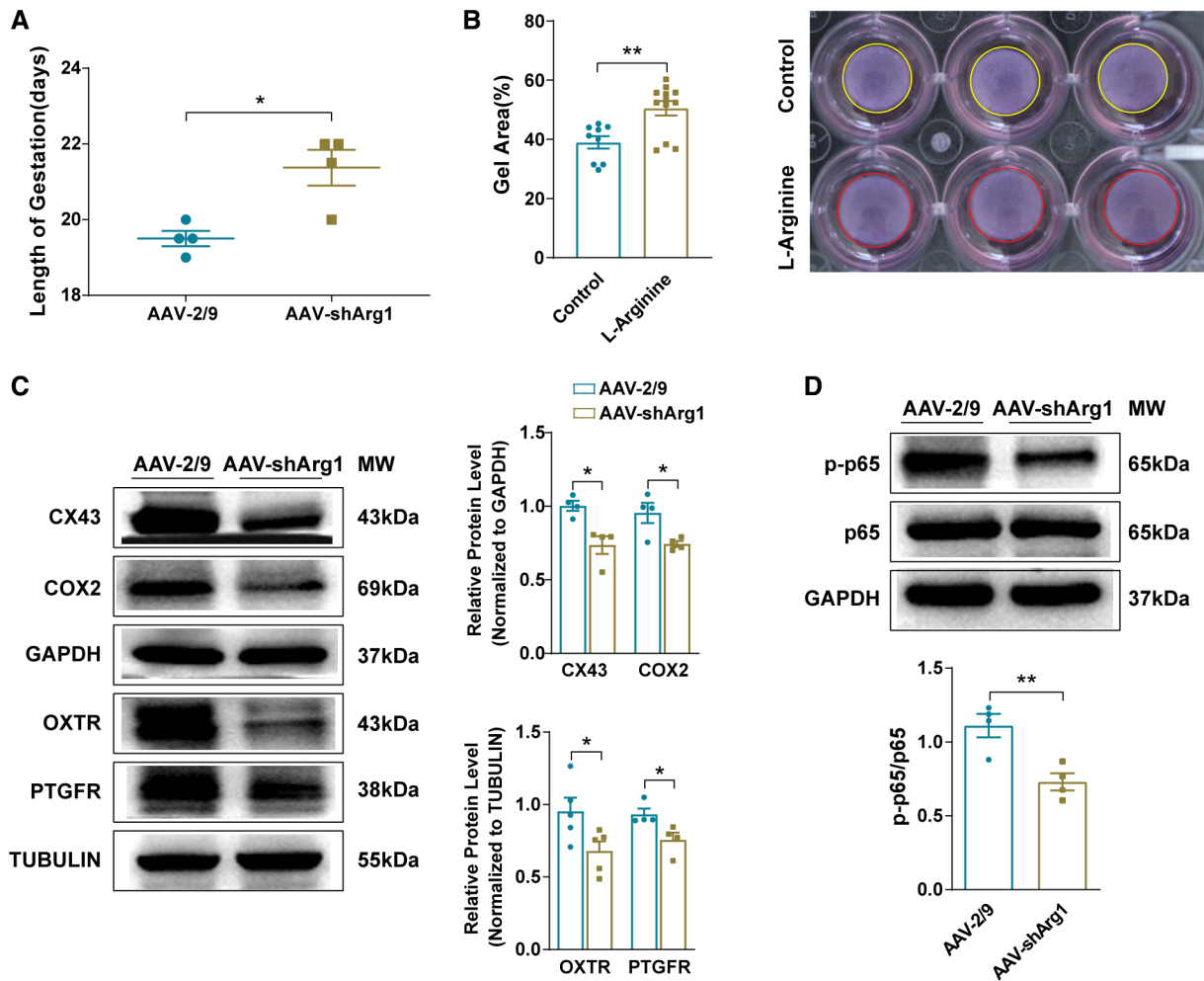


Figure 6. Knockdown of *Arg1* in fetal lungs blocks the activation of NF- κ B and inhibits the expression of downstream CAP-encoding genes in the myometrium.

- A The average gestation length in days of mice injected intraplacentally with AAV-shArg1 or AAV control viruses. Unpaired *t*-test analysis was used and data are the mean \pm s.e.m. of gestation length. $n = 4$ biological replicates per group. $*P < 0.05$.
- B Quantitative analysis of the gel area containing hTERT-HM cells treated with L-arginine or vehicle control. Mann-Whitney test was used to analyze the data, and $n = 9$ biological replicates in control group and $n = 12$ biological replicates in L-Arginine-treated group. The data are shown as the mean \pm s.e.m. $**P < 0.01$. Representative images of spontaneous contractions of the gel disks are shown.
- C Representative western blots and quantitative analysis of CAP expression in the myometrium of pregnant mice injected intraplacentally with AAV-shArg1 or AAV control viruses. Mann-Whitney test was used to analyze CX43 and PTGFR data and unpaired *t*-test was used to analyze COX2 and OXTR data. $n = 4$ biological replicates for CX43, COX2, and PTGFR groups, and $n = 5$ biological replicates for OXTR group. The data are shown as the mean \pm s.e.m. $*P < 0.05$.
- D Representative western blots and quantitative analysis of NF- κ B p-p65 (phospho-S536) and NF- κ B p65 expression in the myometrium of pregnant mice injected intraplacentally with AAV-shArg1 or AAV control viruses. Unpaired *t*-test was used and $n = 4$ biological replicates for each group. The data are shown as the mean \pm s.e.m. $**P < 0.01$.

Source data are available online for this figure.

saccular stage and alveolar stage (Mendelson, 2000; Nikolic et al, 2018). Except for the alveolar stage, which is completed after birth, the first four stages occur *in utero* (Surate Solaligie et al, 2017). Angiogenesis and the development of the pulmonary vascular system are generally considered to be factors that drive alveolar formation (Mariduena et al, 2022). After birth, ARG1 inhibition can increase the bioavailability of L-arginine, restore normal pulmonary vascular resistance and middle wall thickness, and improve the structure and function of pulmonary blood vessels in

young rats (Surate Solaligie et al, 2017). However, in the present study, we found that decreased ARG1 expression and increased L-arginine level were associated with abnormal fetal lung development, suggesting that ARG1 and its metabolites may play different roles in the intrauterine stage of fetal lung development compared with their roles after birth (Lewin & Hurtt, 2017).

In addition to being an important substrate for protein synthesis, arginine is also a precursor of many molecules related to cell signaling and metabolic functions, including NO, proline, and polyamines

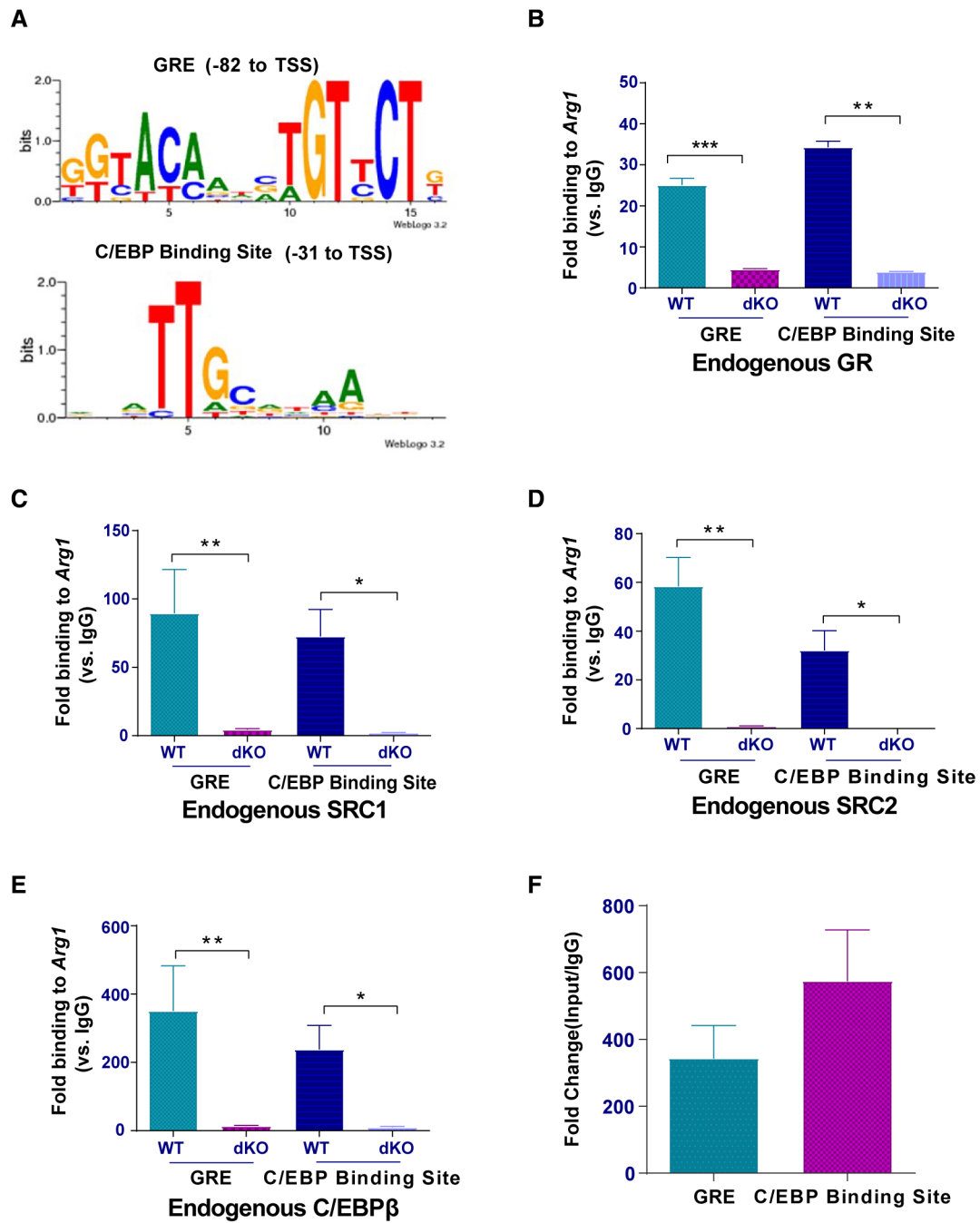


Figure 7. GR and C/EBPβ enhance *Arg1* promoter transactivation in an SRC-1/SRC-2-dependent manner.

A Consensus motifs containing putative GRE and C/EBP-binding sites in the mouse *Arg1* promoter between -1,000 and 0 bp relative to transcription start site (TSS).
 B-E Chromatin immunoprecipitation (ChIP) was performed with WT or *Src-1/-2* dKO fetal lung tissues using antibodies against GR (B), SRC-1 (C), SRC-2 (D), or C/EBPβ (E). Enrichment of these transcription factors at the GRE- or C/EBP-binding sites within the *Arg1* promoter were determined by quantitative PCR. Unpaired *t*-test was used for panel (B) and Mann-Whitney test was used for Panel (C-E). *n* = 6 biological replicates for each group. The data are presented as the mean ± s.e.m. **P* < 0.05, ***P* < 0.01, and ****P* < 0.001.
 F Quantitative PCR results for GRE- and C/EBP-binding site using “input” (positive control) DNA without being immunoprecipitated with any specific antibody. *n* = 6 biological replicates for each group. The data are presented as the mean ± s.e.m.

Source data are available online for this figure.

(Wu & Morris, 1998; Wu et al, 2013; Herring et al, 2018; Hsu & Tain, 2019; Weckman et al, 2019), which play important roles in pregnancy and fetal development. NO can increase placental blood flow (Hou et al, 2016; Weckman et al, 2019) and participate in many processes during pregnancy (Sutton et al, 2020). The intravenous administration of 20 g/day of L-arginine for seven consecutive days to women in the third trimester of pregnancy was found to increase the weight of newborns with unexplained IUGR, possibly by increasing the bioavailability of NO to the fetus (Wu et al, 2012). Although by RNA-seq, we observed that NO synthase expression in the lungs of *Src-1/-2*-deficient fetuses was similar to WT, metabolomics analysis revealed that the concentration of ADMA in the lungs of *Src-1/-2*-deficient fetuses was increased compared to that of WT. ADMA is the most powerful endogenous competitive inhibitor of NO synthase. ADMA is derived from the catabolism of post-translationally modified proteins containing methylated arginine residues (Jarquin Campos et al, 2019) and competes with L-arginine for the active site of NO synthase to inhibit NOS activity (Luiking et al, 2012). The accumulation of ADMA during pregnancy may affect fetal development by interfering with placental vascular endothelial function and angiogenesis (Dai et al, 2020).

In nonhepatic tissues lacking a complete urea cycle, the ARG1 reaction is considered to be a source of ornithine, which leads to the production of other bioactive molecules, such as polyamines (spermine and spermidine), proline, or glutamic acid (Bjelakovic et al, 2015; Sivashanmugam et al, 2017). Proline is a major component of many structural proteins, especially collagen (Caldwell et al, 2018). Polyamines can interact with RNA and DNA to regulate protein synthesis and cell growth and play an important role in the normal growth of the placenta and fetus (Igarashi & Kashiwagi, 2010). In the present study, we also found that the concentration of ornithine was significantly decreased in the *Src-1/-2* dKO fetal lungs, suggesting that the production of downstream ornithine metabolites may be inhibited. Whether paradoxical intrauterine fetal lung dysplasia after *Arg1* knockdown is attributed to the increased ADMA-to-NO ratio or caused by the decreased production of ornithine and its downstream metabolites, proline and polyamines, remains to be determined.

A series of studies have shown that arginine levels are related to the initiation of labor (Neri et al, 2010). A prospective cohort study showed that maternal arginine intake was negatively correlated with overall preterm births and preterm births that occurred before 34 weeks of gestation (Darling et al, 2017). When the intake of arginine reached approximately 1,500 mg/1,000 kcal, the rate of preterm delivery before 34 weeks was significantly reduced (Darling et al, 2017). Moreover, the experimental administration of arginine to pregnant women at risk of preterm birth significantly increased the length of gestation (Neu, 2009; Winer et al, 2009; Neri et al, 2010) and lowered the preterm birth rate (Vadillo-Ortega et al, 2011). In the present study, we found that reduced expression of *Arg1* in fetal lungs was associated with a delay in the timing of parturition in pregnant mice. Since ARG1 expression was not changed in maternal myometrium, we proposed that the accumulation of arginine in fetal lungs due to the deficiency of *Arg1* may inhibit the contraction of myometrium in an endocrine manner or a paracrine manner (through secretion into the amniotic fluid). This hypothesis is supported by the findings that L-arginine exerts an inhibitory effect on the contraction of uterine strips from pregnant rats (Izumi

et al, 1993; Yallampalli et al, 1994), of uteri from pregnant dogs near term (Rizzo et al, 2011), and in women at risk of premature labor (Facchinetti et al, 1996). Furthermore, this is consistent with our observations that L-arginine significantly inhibited spontaneous contractions of the human myometrial smooth muscle cells in culture.

L-arginine may have direct or indirect effects on the contractility of myometrium. The intake of arginine from the diet may increase the bioavailability of NO, thereby reducing the risk of preterm birth (Wu et al, 2012). The competitive NO synthase inhibitor L-nitroarginine methyl ester (L-NAME) can induce preterm labor, which can be prevented by the NO precursor sodium nitroprusside (SNP) (Tiboni & Giampietro, 2000). It was found that NO plays a role in maintaining uterine muscle quiescence by promoting CX43 nitrosylation and weakening gap junction activity (Barnett et al, 2021). In the present study, we found that the addition of L-arginine to culture medium surrounding hTERT-HSMC cells inhibited the expression of various CAPs, including CX43, OXTR, COX2, and PTGFR; this was associated with decreased activation of NF- κ B. Whether L-arginine attenuates NF- κ B activation through protein nitrosylation by increasing the production of NO warrants further investigation.

Arg1 expression was reported to be regulated by a number of transcription factors. The glucocorticoid receptor (GR) can affect the urea cycle in the liver by increasing *Arg1* expression, which contributes to amino acid homeostasis under conditions of glucocorticoid excess (Okun et al, 2015). Studies in rat hepatoma cells have shown that the upregulation of *Arg1* expression by glucocorticoid requires the increased expression of the transcription factor CCAAT/enhancer-binding protein β (C/EBP β), which then binds to the enhancer region spanning the junction of intron 7 and exon 8 of the rat *Arg1* promoter (Gotoh et al, 1997). In macrophages, C/EBP β deficiency inhibits the expression of *Arg1* (Larabee et al, 2018). Interestingly, our recent studies revealed that the expression of C/EBP β was reduced in the lungs of *Src-1/-2* dKO fetuses. Further, glucocorticoids induced C/EBP α and C/EBP β expression, whereas GR, SRC-1, and SRC-2 binding was only evident at the C/EBP β promoter but not detectable in the C/EBP α promoter in lung tissues of WT fetal mice (Chen et al, 2020). Collectively, these results suggested that the GC-induced C/EBP β expression is essential for the transcriptional activation of *Arg1* in mouse fetal lung.

Unlike rats, we found in the present study that the C/EBP β -binding site exists in the promoter region upstream from the transcription start site of mouse *Arg1* gene, and is quite proximal to the glucocorticoid-responsive element (GRE). Moreover, ChIP-seq and ChIP-on-Chip assays have shown that in liver tissue, GR was exclusively associated with accessible chromatin, and 62% of GR-binding sites were occupied by C/EBP β . Disruption of C/EBP β binding to chromatin resulted in attenuation of GR recruitment and GR-induced chromatin remodeling specifically at sites co-occupied by GR and C/EBP β (Phuc Le et al, 2005; Grontved et al, 2013). On the other hand, there is evidence that GR binds to C/EBP β response elements through a tethering mechanism to mediate GC induction of MKP-1/DUSP1 gene expression (Johansson-Haque et al, 2008). Similarly, in the present study, we found that endogenous GR and C/EBP β can not only bind to their individual response element but also bind to each other's putative binding site. These results demonstrated a highly cooperative mechanism by which GR and C/EBP β reciprocally regulated selective and tethered C/EBP β and GR binding to the promoter of *Arg1* in an SRC-1/SRC-2-dependent manner.

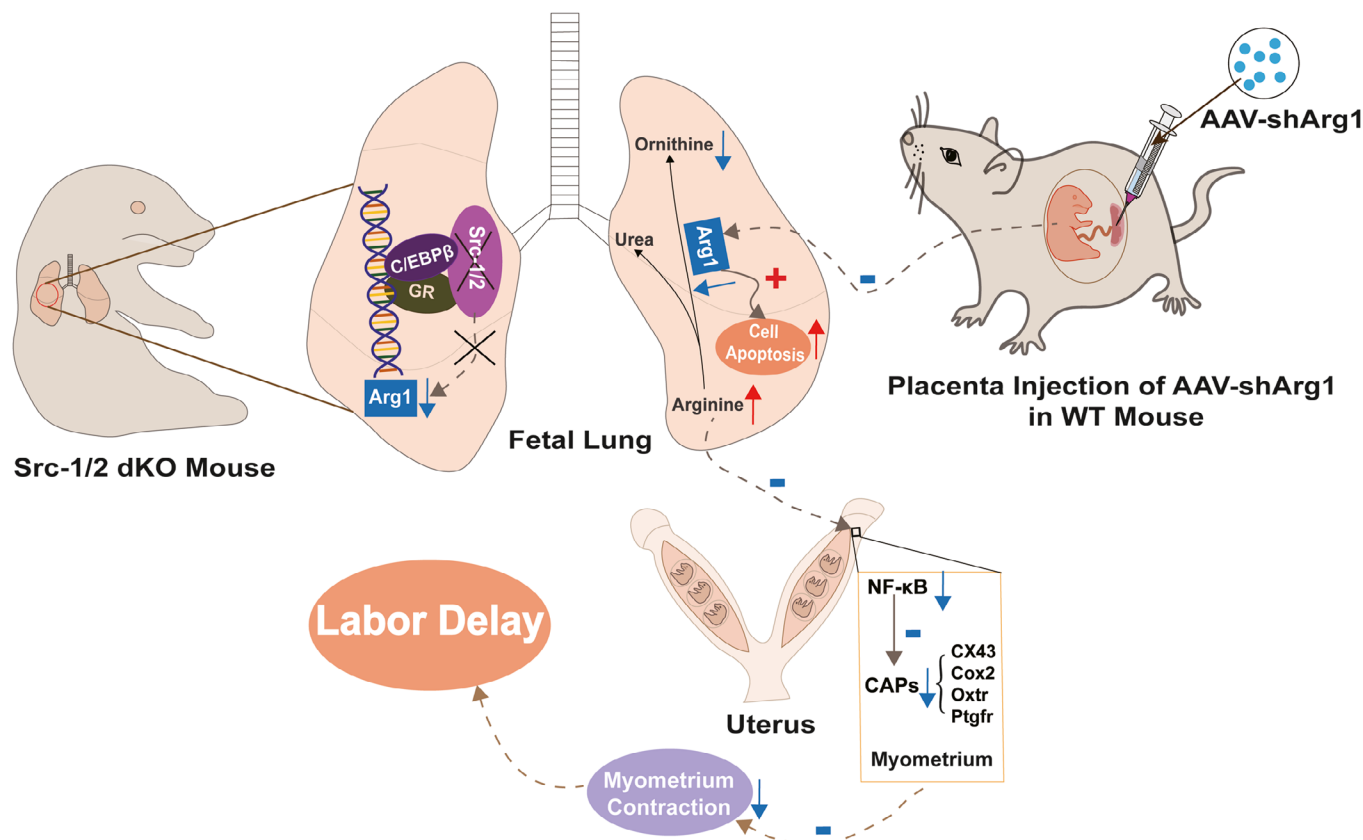


Figure 8. Schematic diagram of the regulation of Arg1 and its roles in fetal lung development and parturition.

GR and C/EBP β increase transcription of Arg1 in an SRC-1/SRC-2-dependent manner by binding to a tethered GRE- and C/EBP-binding site element in the Arg1 promoter. Knockdown of Arg1 in the fetal lung induces apoptosis of epithelial cells and causes the accumulation of the Arg1 substrate arginine. In an endocrine or paracrine manner, arginine significantly inhibits spontaneous myometrial contraction by attenuating the activation of NF- κ B and the expression of downstream genes encoding contraction-associated proteins, which delays the initiation of parturition.

In addition to GR and C/EBP β , the transcription factors Fos-related antigen 1 (Fra-1) and jun proto-oncogene (c-Jun) have been found to be negative regulators of Arg1 transcription (Singh et al, 2014; Hannemann et al, 2019). Whether glucocorticoids/GR acting together with SRC-1 and SRC-2 enhance transcription of Arg1 in the fetal lung by negatively regulating the action of these inhibitory transcription factors is of great interest and will be examined in future studies.

Conclusion

The expression of a key enzyme in arginine metabolism, ARG1, is developmentally upregulated in fetal lungs during late gestation and is significantly decreased in Src-1/-2 dKO mice. The lungs of these mice also exhibited increased levels of the ARG1 substrate L-arginine and decreased levels of the ARG1 metabolite ornithine. Knockdown of Arg1 in the fetal lung increased the levels of L-arginine, which induced apoptosis of fetal lung epithelial cells and dramatically delayed the initiation of parturition (Fig 8). Compared with our previous findings in Src-1/-2 dKO mice, we suggest that Arg1 and its metabolite L-arginine are more important for the

development and maturation of fetal lung, while SP-A and DPPC are more important for the preparation of air breathing of the fetus after birth. All of these fetus-derived factors may comprehensively act as signals and contribute to the initiation of labor. This finding again supports the hypothesis that parturition is a complex maternal-fetal crosstalk, and multiple fetal lung-derived factors may be involved in this process and serve as link among fetal lung development, functions, and parturition.

Materials and Methods

Animal models

All animal procedures were approved by the Animal Care and Use Committee of Naval Medical University, Shanghai (ethics approval number: 20210308001). All the animal care and treatments were carried out in compliance with Naval Medical University Animal Care. Src-1^{-/-} mice and Src-2^{+/-} mice were obtained from our in-house stock. Src-1^{+/-}/Src-2^{+/-} mice were generated by crossing Src-1^{-/-} mice with Src-2^{+/-} mice and were subsequently bred to generate Src-1^{-/-}/Src-2^{+/-} males and females. C57BL/6J wild-type

(WT) mice were purchased from Shanghai Regan Corporation, Shanghai, China. WT females were bred to WT males as controls. Breeding pairs were placed in the same cage at 6:00 pm and separated at 8:00 am the next day; gestational age was considered 0.5 dpc when a vaginal plug was observed. The time of labor was defined as delivery of the first pup. All the mice were bred in a housing condition with a 12-h-dark/12-h-light cycle and were pathogen free, and the mice were allowed free access to standard pellet chow.

For genotyping, DNA was extracted from the tails of mice using a Mouse Tail Kit (Foregene, Chengdu, China) and amplified by PCR, and genotyping was performed as previously described (Gao et al, 2015). PCR products were size fractionated on 2% agarose gels and visualized with ethidium bromide.

Collection of fetal lungs

Pregnant females were euthanized by cervical dislocation. Fetal lungs were harvested from timed-pregnant mice at approximately 10:00 am at 15.5 dpc, 16.5 dpc, 17.5 dpc, 18.5 dpc, and labor. All the tissues were washed with ice-cold 1× PBS, frozen immediately in liquid nitrogen, and then stored at -80°C until analysis. Tails of fetuses from *Src*-deficient females were stored at -20°C for subsequent DNA isolation and genotyping.

RNA sequencing

RNA sequencing of fetal lungs was previously described (Chen et al, 2020). Briefly, total RNA was extracted from the lungs of WT, *Src1*^{-/-} (*Src1* KO), *Src2*^{-/-} (*Src2* KO), and *Src1/Src2* (dKO) fetuses (four samples in each group) at 18.5 dpc. After RNA purity and integrity were assessed, 2 μg of total RNA per sample was extracted and used for cDNA library construction. Transcriptome sequencing was carried out on an Illumina HiSeq platform. After removing low-quality sequences and contaminants from the 150-bp paired-end (PE) raw reads, the high-quality sequences (clean reads) were subsequently analyzed. Differential gene expression was identified between sample groups by applying the R package DESeq2. A gene was considered a DEG when it met the following criteria: twofold cutoff change (\log_2 -fold change > 1) in transcript levels and *q* (adjusted *P*) value < 0.05. GO analysis and KEGG datasets were used to calculate the significance of the enrichment of DEGs in each pathway.

Reverse transcriptase quantitative PCR

Total RNA was extracted from fetal lungs using the TRIzol method. Quantitation of total RNA was performed by Microplate readers (Biotek, USA). Then, 0.6 μg of total RNA was reverse transcribed using a PrimeScript RT reagent Kit with gDNA Eraser (Takara, Japan). Gene expression levels were quantified by a CFX Connect Real-Time System (Bio-Rad, USA) using Thunderbird qPCR Mix (Toyobo, Taiwan, China). β-actin expression was measured in parallel for normalization. The cycling conditions were 95°C for 1 min, followed by 49 cycles of 95°C for 15 s and 60°C for 1 min. The specificity of the primers was verified by examining the melting curve. Distilled water was used in place of cDNA as a negative control for all the reactions. Each sample was amplified in triplicate, and the

mean C_q value was calculated. The abundance of mRNA was quantified using the $2^{-\Delta\Delta C_t}$ method. The primer sequences are illustrated in Table EV1.

Western blotting

Tissues were lysed in RIPA lysis buffer (Solarbio, Beijing, China) supplemented with protease inhibitors (Abcam, UK) to extract total protein. Proteins were separated on 10% SDS-PAGE gels and transferred to PVDF membranes (Millipore, UK). The membranes were blocked with 5% nonfat milk for 2 h and incubated overnight at 4°C with antibodies against ASS1 (PA5-18679, 1:1,000, Thermo Scientific, USA), ARG1 (ab233548, 1:1,000, Abcam), Ki67 (ab16667, 1:1,000, Abcam), CASPASE3 (9,662, 1:1,000, CST, USA), COX2 (ab15191, 1:1,000, Abcam), PTGFR (PA5-110237, 1:1,000, Thermo Scientific), CX43 (ab11370, 1:2,000, Abcam), OXTR (ab181077, 1:1,000, Abcam), NF-κB p65 (ab32536, 1:1,000, Abcam), NF-κB p-p65 (ab76302, 1:1,000, Abcam), TUBULIN (ab7291, 1:1,000, Abcam), and β-ACTIN (ab8226, 1:1,000, Abcam). Immunoreactive bands were visualized using Peroxidase-AffiniPure Goat Anti-Mouse IgG (115-035-020, 1:5,000, Jackson, USA) or Peroxidase-AffiniPure Goat Anti-Rabbit IgG (111-035-045, 1:5,000, Jackson) and ECL solution (Thermo Scientific), and the bands were subsequently analyzed using the Tanon 5,200 chemiluminescent imaging system. The immunoblots were quantified using ImageJ software. Relative protein expression levels were normalized to the corresponding β-actin or tubulin expression level as a loading control.

Immunohistochemistry

Fetal lung tissues were fixed in 4% paraformaldehyde for 24 h and embedded in paraffin after dehydration. Sections (5 μm) were deparaffinized, rehydrated, and boiled for 15 min in 10 mM citrate buffer (pH 6). Nonspecific background staining was blocked by incubation with 3% hydrogen peroxide (Sigma, USA) at room temperature for 25 min in the dark. The sections were blocked in 3% bovine serum albumin (BSA) for 30 min and then incubated at 4°C overnight with primary antibody against ARG1 (ab233548, 1:50, Abcam), ASS1 (PA5-18679, 1:150, Thermo Scientific), or PBS (negative control). The following day, the sections were incubated with horseradish peroxidase-conjugated secondary antibody (GK500705, GeneTech, Shanghai, China) at room temperature for 40 min. The bound antibodies were detected using one drop of DAB chromogenic agent to 1 ml of DAB buffer (GeneTech). Nuclei were counterstained using a hematoxylin counterstain reagent (Servicebio, Wuhan, China). The sections were then dehydrated and analyzed using a Nikon Digital Sight DS-Fi2 microscope.

LC-MS and MRM analysis of amino acids

Twenty milligrams of fetal lung tissues were homogenized with 200 μl of water. Then, 800 μl methanol acetonitrile solution (1:1, v/v) was added, and the samples were sonicated at 4°C for 30 min twice. Proteins in the homogenates were precipitated at -20°C for 1 h. The homogenized samples were centrifuged at 4°C for 15 min, and the supernatants were dried and stored at -80°C until analysis.

LC-MS analysis was performed using a UHPLC system (Waters I-class, Waters, Germany) coupled to a triple quadruple mass

spectrometer (AB 5500 QTRAP, AB SCIEX, USA) in multiple reaction monitoring (MRM) mode. Samples were separated using a 2.1 mm × 100 mm ACQUITY UPLC BEH 1.7 μm column (Waters). Mobile phase A was 25 mM ammonium acetate and 25 mM ammonia in water (pH 9.75), and mobile phase B was acetonitrile. The gradient elution profile was t = 1 min, 95% B; t = 14 min, 65% B; t = 18 min, 40% B; t = 18.1 min, 95% B, and t = 23 min, 95% B. The flow rate was 300 μl/min, and the injection volume was 2 μl. The temperature of the column was maintained at 40°C, and the autosampler was chilled at 4°C. QC samples were injected after every six sample runs to monitor the quality of the LC–MS. The MS conditions were set as follows: sheath gas temperature, 350°C; dry gas temperature, 350°C; sheath gas flow, 11 l/min; dry gas flow, 10 l/min; capillary voltage, 4,000 V or –3,500 V in positive or negative modes, respectively; nozzle voltage, 500 V; and nebulizer pressure, 30 psi. Two hundred metabolites, including amino acids, in the samples were monitored in MRM mode. The dwell time for each MRM ion pair was 3 ms, and the total cycle time was 1.263 s. MRM raw data were extracted by MRM analyzer (R), and the analysis was conducted following a previously described method (Cai *et al*, 2015). To investigate the significance of the metabolites observed by LC–MS–MRM, KEGG (Kyoto Encyclopedia of Genes and Genomes) pathway analysis was performed.

A549 cell culture and treatment

A549 cells (lung adenocarcinoma cell line) were plated into 24-well culture plates in a culture medium containing 10% FBS and 1% penicillin–streptomycin under standard tissue culture conditions for 24 h. Then, the cells were incubated with L-arginine (Merck, A8094) at a final concentration of 0.1 mg/ml for 24 h. A549 cells were collected from each treatment with three biological replicates for TUNEL assay (Beyotime, C1090).

Generation of AAV-shArg1 and placental injection

The adeno-associated virus pAAV2/9-U6-GFP vector carrying either the shRNA control sequence (TTCTCCGAACGTGTCACGT) or *shArg1* sequence (GGAAGTGAACCAACTCTTGG) was designed and generated by Genomeditech (Shanghai, China).

Timed-pregnant C57BL/6J WT mice were anesthetized with isoflurane via a precision vaporizer at 13.0 dpc. The fur covering the abdominal region was shaved, and an incision was made to expose the uterine horns. Each placenta in both uterine horns was injected with 5 μl of AAV-shArg1 (5×10^{12} VG/ml) or AAV-2/9 (control, 5×10^{12} VG/ml) particles using microsyringes (Gaoge Tech Company, Shanghai); all placentas in the same female were injected with the same particles. After the operation, uterine horns were returned to the abdominal cavity, and the incision was sutured. The mice were kept on a warming pad and returned to their cages after recovery from the surgery. The mice were allowed to deliver to analyze the parturition timing or sacrificed at labor to harvest the fetal lungs, fetal livers, placentas, and myometrium. To precisely determine the time to labor, since 18.5 dpc, the mouse cage was monitored every half hour from 7:00 am to 12:00 pm and every hour from 12:00 pm to 6:00 am, and the delivery of the first pup was documented as the time to labor.

Preparation of frozen sections

To verify whether the AAV successfully infected the tissues, samples were fixed in 4% paraformaldehyde for 24 h and dehydrated in 30% sucrose solution overnight. Then, the samples were snap-frozen in optimal cutting temperature compound and sectioned at 5 μm. The slides were incubated at 37°C for 15 min and subsequently photographed using a Nikon Eclipse Ti fluorescence microscope to observe GFP expression.

Immunofluorescence

Fetal lung sections were prepared as mentioned above. After deparaffinization and rehydration, antigen retrieval was performed by boiling in 10 mM citrate buffer (pH 6). The slides were blocked in BSA for 30 min and stained with Ki67 antibody (ab16667, 1:500, Abcam) at 4°C overnight. The next day, Cy3 AffiniPure goat anti-rabbit IgG (K1034G-Cy3, 1:300, Servicebio) was added to the slides and incubated at room temperature for 40 min.

In multiplex fluorescent immunohistochemistry, all the steps were the same as described above until the primary antibody was added. The slides were incubated with primary antibodies against ARG1 (16001-1-AP, 1:500, Proteintech, USA) or ASS1 (PA5-18679, 1:150, Thermo Scientific), followed by the application of the Cy3 AffiniPure Goat Anti-Rabbit IgG (K1034G-Cy3, 1:300, Servicebio) secondary antibody. After pipetting 100 μl TSA-Cy3 working solution from the TSA Fluorescence Palette Kit (Servicebio) onto the slides to amplify the signal, the slides were again boiled in citrate buffer to strip the primary/secondary antibody complexes and were ready for labeling of LPCAT1 antibody (16112-1-AP, 1:300, Proteintech) and PDPN antibody (ab11936, 1:200, Abcam). Cy5 AffiniPure Goat Anti-Rabbit IgG (K0034G-Cy5, 1:300, Servicebio) or Goat Anti-Syrian Hamster IgG H&L (ab180063, 1:500, Abcam) was added to slides as a secondary antibody. Then, 100 μl TSA-Cy5 working solution was added to the slides. Nuclear DNA was labeled with DAPI, and the slides were mounted with Fluoromount. The stained slides were analyzed using a Nikon Eclipse Ti fluorescence microscope.

TUNEL assay

Paraffin-embedded fetal lung sections were deparaffinized, rehydrated, and incubated with proteinase K at 37°C for 20 min to retrieve the antigens. The cell membrane was permeabilized with Triton X-100. Apoptotic fetal lung epithelial cells were observed with TUNEL staining (red signals) according to the manufacturer's instructions. For multiplex fluorescent immunohistochemistry, the slides were labeled with LPCAT1 antibody (16112-1-AP, 1:300, Proteintech) or PDPN antibody (ab11936, 1:200, Abcam). Cy5 AffiniPure Goat Anti-Rabbit IgG (GB27301, 1:300, Servicebio) or Goat Anti-Syrian Hamster IgG H&L (ab180063, 1:500, Abcam) was added to slides as a secondary antibody. Then, 100 μl TSA-Cy5 working solution was added to the slides. To determine the number of nuclei, the slides were incubated with DAPI for 10 min at 37°C in the dark and washed with PBS (pH 7.4) three times for 5 min each. Then, the slides were mounted with antifade Fluoromount. Images were obtained using a Nikon Eclipse Ti fluorescence microscope. Quantitative analysis of the TUNEL fluorescence intensity was performed with ImageJ software. Three random fields of view

occupied by the fetal lung in each image were defined manually, and the mean fluorescence intensity of the signal within these areas was measured.

Collagen matrix contractility assay

Immortalized hTERT human myometrial smooth muscle cells (hTERT-HMSMCs) were generated from primary culture of human myometrial cells infected with expression vectors containing the human telomerase reverse transcriptase (hTERT), according to the previous publication (Condon *et al*, 2002). hTERT-HMSMCs were combined with type I rat tail collagen solution (3 mg/ml, catalog no. 356236; BD Biosciences, USA) to achieve a density of 1×10^5 cells per gel with a final collagen concentration of 1.0 mg/ml. The collagen gel-cell suspensions were pipetted into wells of a 24-well culture plate immediately after NaOH (3 μ l/gel) was added and incubated for 30 min at room temperature to allow polymerization. One milliliter of fresh DMEM, either not supplemented (control) or supplemented with L-arginine (0.1 mg/ml) or ornithine (0.1 mg/ml), was added over the cell-collagen matrix. The gel was then detached from its mold by gently running a 10 μ l pipet tip around the gel edges. Images of the floating gels were captured at 24 h after treatment, and the area of each gel was measured using ImageJ software.

ChIP-qPCR

Fetal lung tissues isolated from WT and *Src-1/-2* dKO fetuses at 18.5 dpc were finely minced and immediately incubated in 1% formaldehyde for 15 min at room temperature. The pelleted tissues were washed, resuspended in SDS lysis buffer supplemented with a protease inhibitor cocktail, and then sonicated. Sheared chromatin was diluted in ChIP dilution buffer with Dynabeads™ Protein G (Millipore, CS200638) and incubated with anti-GR (Cell Signaling, Cat No. 12041, USA), anti-SRC-1 (Bethyl Laboratories, A300-344A, USA), anti-SRC-2 (Bethyl Laboratories, A300-346A), anti-C/EBP β (Abcam, ab32358), or mouse IgG (Millipore, 12-371B) antibodies at 4°C overnight. The beads were washed following the manufacturer's instructions (Millipore, 17-20000). Crosslinking was reversed by incubation with ChIP Elution Buffer/Prok at 62°C for 2 h with shaking. DNA was then extracted from the samples using phenol/chloroform. RT-qPCR was performed using primer pairs (listed in Table EV1) to amplify putative binding sites of GR and C/EBP β in the promoter of *Arg1* at -82 and -31 upstream to transcriptional starting site, respectively. The primers were designed carefully to make sure that each primer pair only pick up one specific binding site and avoid the nonspecific amplification of the adjacent binding site. The fold binding is calculated with the expression of GRE- or C/EBP-binding site from the chromatin DNA immunoprecipitated with specific antibody versus the expression of GRE- or C/EBP-binding site from the chromatin DNA immunoprecipitated with IgG.

Statistics

No statistical methods were used to predetermine sample size, and the investigators were not blinded to outcome assessment. All the statistical analyses were performed with Graphpad Prism software. Normality test was performed on all data, and one-way ANOVA followed by Tukey's multiple-comparison test or unpaired Student's

t-test was employed if the data follow normal distribution; if the data did not follow normal distribution, we used nonparametric methods (Kruskal–Wallis test or Mann–Whitney test) to analyze the data. Unless otherwise stated, all the data are shown as the mean \pm s.e.m. $P < 0.05$ was considered statistically significant.

Data availability

The datasets produced in this study are available in the following databases:

RNA-Seq Data: Figshare. Dataset. <https://doi.org/10.6084/m9.figshare.22589926.v3>.

Targeted Metabolomics Data: Figshare. Dataset. <https://doi.org/10.6084/m9.figshare.22587187.v5>.

Expanded View for this article is available [online](#).

Acknowledgements

The authors would like to acknowledge Applied Protein Technology Company for the LC–MS and MRM analyses of amino acids. Research in the Gao laboratory is supported by National Key Research and Development Project 2022YFC2704602 and 2022YFC2704502, National Natural Science Foundation of China 82120108011, Major Project of Shanghai Municipal Education Commission's Scientific Research and Innovation Plan 2021-01-07-00-07-E00144, and Strategic Collaborative Research Program of the Ferring Institute of Reproductive Medicine FIRMA200502. CRM is supported by NIH grants R01-HL050022 and P01-HD087150, and Burroughs Wellcome Preterm Birth Grant 1019823. The graphical abstract for this article was created using BioRender via a subscription maintained by YYL. I personally would like to dedicate this article to Dr. Carole Mendelson at the University of Texas Southwestern Medical Center, a prestigious scientist in the area of reproductive sciences, the former President of the Society for Reproductive Investigation, and a long-lasting mentor and collaborator of mine. She gave a lot of suggestions and advices during this project and manuscript preparation before she passed away on Feb. 12, 2023. Hereby, I would like to express my most sincere respect and deepest remembrance to her.

Author contributions

Yaqin Yu: Formal analysis; investigation; visualization; methodology; writing – original draft. **Yuanyuan Liu:** Investigation; visualization; methodology. **Xuesong Sui:** Formal analysis; investigation; visualization; methodology. **Yanyu Sui:** Investigation; methodology. **Zhe Wang:** Formal analysis; visualization. **Carole R Mendelson:** Conceptualization; funding acquisition; writing – review and editing. **Lu Gao:** Conceptualization; formal analysis; supervision; funding acquisition; investigation; visualization; writing – original draft; project administration; writing – review and editing.

Disclosure and competing interests statement

The authors declare that they have no conflict of interest.

References

- Ayers-Ringler J, Kolumam Parameswaran P, Khashim Z, Dai D, Ding YH, Kallmes DF, Kadirvel R (2021) L-arginine reduces downstream vascular contractility after flow-diverting device deployment: a preliminary study in a rabbit model. *Interv Neuroradiol* 28: 183–189

- Barnett SD, Asif H, Anderson M, Buxton ILO (2021) Novel Tocolytic strategy: modulating Cx43 activity by S-Nitrosation. *J Pharmacol Exp Ther* 376: 444–453
- Bird AD, Choo YL, Hooper SB, McDougall AR, Cole TJ (2014) Mesenchymal glucocorticoid receptor regulates the development of multiple cell layers of the mouse lung. *Am J Respir Cell Mol Biol* 50: 419–428
- Bjelakovic G, Miladinovic P, Jevtovic-Stoimenov T, Stojanovic I, Nikolic J, Pavlovic D, Kocic G, Bjelakovic M, Ilic M, Sokolovic D et al (2015) Arginase activity and lecithin/sphingomyelin (l/s) ratio in the amniotic fluid of pregnant women. *Indian J Clin Biochem* 30: 84–88
- Bjorke-Jenssen A, Ueland PM, Bjorke-Monsen AL (2017) Amniotic fluid arginine from gestational weeks 13 to 15 is a predictor of birth weight, length, and head circumference. *Nutrients* 9: 1357
- Cai Y, Zhu ZJ (2019) A high-throughput targeted metabolomics workflow for the detection of 200 polar metabolites in central carbon metabolism. *Methods Mol Biol* 1859: 263–274
- Cai Y, Weng K, Guo Y, Peng J, Zhu Z-J (2015) An integrated targeted metabolomic platform for high-throughput metabolite profiling and automated data processing. *Metabolomics* 11: 1575–1586
- Caldwell RW, Rodriguez PC, Toque HA, Narayanan SP, Caldwell RB (2018) Arginase: a multifaceted enzyme important in health and disease. *Physiol Rev* 98: 641–665
- Chen J, Mishra R, Yu Y, McDonald JG, Eckert KM, Gao L, Mendelson CR (2020) Decreased 11beta-hydroxysteroid dehydrogenase 1 in lungs of steroid receptor coactivator (Src)-1/-2 double-deficient fetal mice is caused by impaired glucocorticoid and cytokine signaling. *FASEB J* 34: 16243–16261
- Cole TJ, Blendy JA, Monaghan AP, Krieglstein K, Schmid W, Aguzzi A, Fantuzzi G, Hummler E, Unsicker K, Schutz G (1995) Targeted disruption of the glucocorticoid receptor gene blocks adrenergic chromaffin cell development and severely retards lung maturation. *Genes Dev* 9: 1608–1621
- Condon J, Yin S, Mayhew B, Word RA, Wright WE, Shay JW, Rainey WE (2002) Telomerase immortalization of human myometrial cells. *Biol Reprod* 67: 506–514
- Condon JC, Jeyasuria P, Faust JM, Mendelson CR (2004) Surfactant protein secreted by the maturing mouse fetal lung acts as a hormone that signals the initiation of parturition. *Proc Natl Acad Sci USA* 101: 4978–4983
- Dai Y, Zhang J, Liu R, Xu N, Yan SB, Chen Y, Li TH (2020) The role and mechanism of asymmetric dimethylarginine in fetal growth restriction via interference with endothelial function and angiogenesis. *J Assist Reprod Genet* 37: 1083–1095
- Darling AM, McDonald CR, Urassa WS, Kain KC, Mwiru RS, Fawzi WW (2017) Maternal dietary L-arginine and adverse birth outcomes in Dar es Salaam, Tanzania. *Am J Epidemiol* 186: 603–611
- Facchinetti F, Neri I, Genazzani AR (1996) L-arginine infusion reduces preterm uterine contractions. *J Perinat Med* 24: 283–285
- da Fonseca EB, Damiao R, Moreira DA (2020) Preterm birth prevention. *Best Pract Res Clin Obstet Gynaecol* 69: 40–49
- Frenkel RA, Mugeruma K, Johnston JM (1996) The biochemical role of platelet-activating factor in reproduction. *Prog Lipid Res* 35: 155–168
- Fuchs F, Senat MV (2016) Multiple gestations and preterm birth. *Semin Fetal Neonatal Med* 21: 113–120
- Gao L, Rabbitt EH, Condon JC, Renthal NE, Johnston JM, Mitsche MA, Chambon P, Xu J, O'Malley BW, Mendelson CR (2015) Steroid receptor coactivators 1 and 2 mediate fetal-to-maternal signaling that initiates parturition. *J Clin Invest* 125: 2808–2824
- Glover AV, Manuck TA (2018) Screening for spontaneous preterm birth and resultant therapies to reduce neonatal morbidity and mortality: a review. *Semin Fetal Neonatal Med* 23: 126–132
- Gotoh T, Chowdhury S, Takiguchi M, Mori M (1997) The glucocorticoid-responsive gene cascade. Activation of the rat arginase gene through induction of C/EBPbeta. *J Biol Chem* 272: 3694–3698
- Grontved L, John S, Baek S, Liu Y, Buckley JR, Vinson C, Aguilera G, Hager GL (2013) C/EBP maintains chromatin accessibility in liver and facilitates glucocorticoid receptor recruitment to steroid response elements. *EMBO J* 32: 1568–1583
- Hannemann N, Cao S, Eriksson D, Schnelzer A, Jordan J, Eberhardt M, Schleicher U, Rech J, Ramming A, Uebe S et al (2019) Transcription factor Fra-1 targets arginase-1 to enhance macrophage-mediated inflammation in arthritis. *J Clin Invest* 129: 2669–2684
- Herring CM, Bazer FW, Johnson GA, Wu G (2018) Impacts of maternal dietary protein intake on fetal survival, growth, and development. *Exp Biol Med (Maywood)* 243: 525–533
- Hou Y, Yao K, Yin Y, Wu G (2016) Endogenous synthesis of amino acids limits growth, lactation, and reproduction in animals. *Adv Nutr* 7: 331–342
- Hsu CN, Tain YL (2019) Impact of arginine nutrition and metabolism during pregnancy on offspring outcomes. *Nutrients* 11: 1452
- Igarashi K, Kashiwagi K (2010) Modulation of cellular function by polyamines. *Int J Biochem Cell Biol* 42: 39–51
- Iyer RK, Yoo PK, Kern RM, Rozengurt N, Tsoa R, O'Brien WE, Yu H, Grody WW, Cederbaum SD (2002) Mouse model for human arginase deficiency. *Mol Cell Biol* 22: 4491–4498
- Izumi H, Yallampalli C, Garfield RE (1993) Gestational changes in l-arginine-induced relaxation of pregnant rat and human myometrial smooth muscle. *Am J Obstet Gynecol* 169: 1327–1337
- Jarquín Campos A, Risch L, Baumann M, Purde MT, Neuber S, Renz H, Mosimann B, Raio L, Mohaupt M, Surbek D et al (2019) Shrunken pore syndrome, preeclampsia, and markers of NO metabolism in pregnant women during the first trimester. *Scand J Clin Lab Invest* 79: 91–98
- Johansson-Haque K, Palanichamy E, Okret S (2008) Stimulation of MAPK-phosphatase 1 gene expression by glucocorticoids occurs through a tethering mechanism involving C/EBP. *J Mol Endocrinol* 41: 239–249
- Koullali B, Oudijk MA, Nijman TA, Mol BW, Pajkrt E (2016) Risk assessment and management to prevent preterm birth. *Semin Fetal Neonatal Med* 21: 80–88
- Larabee JL, Hauck G, Ballard JD (2018) Unique, intersecting, and overlapping roles of C/EBP beta and CREB in cells of the innate immune system. *Sci Rep* 8: 16931
- Lewin G, Hurtt ME (2017) Pre- and postnatal lung development: an updated species comparison. *Birth Defects Res* 109: 1519–1539
- Liang L, Rasmussen MH, Piening B, Shen X, Chen S, Röst H, Snyder JK, Tibshirani R, Skotte L, Lee NC et al (2020) Metabolic dynamics and prediction of gestational age and time to delivery in pregnant women. *Cell* 181: e1615
- Liu L, Oza S, Hogan D, Chu Y, Perin J, Zhu J, Lawn JE, Cousens S, Mathers C, Black RE (2016) Global, regional, and national causes of under-5 mortality in 2000–15: an updated systematic analysis with implications for the sustainable development goals. *Lancet* 388: 3027–3035
- Lonard DM, O'Malley BW (2007) Nuclear receptor coregulators: judges, juries, and executioners of cellular regulation. *Mol Cell* 27: 691–700
- Luiking YC, Ten Have GA, Wolfe RR, Deutz NE (2012) Arginine de novo and nitric oxide production in disease states. *Am J Physiol Endocrinol Metab* 303: E1177–E1189
- Mariduena J, Ramagopal M, Hiatt M, Chandra S, Laumbach R, Hegyi T (2022) Vascular endothelial growth factor levels and bronchopulmonary dysplasia in preterm infants. *J Matern Fetal Neonatal Med* 35: 1517–1522
- Mark M, Yoshida-Komiya H, Gehin M, Liao L, Tsai MJ, O'Malley BW, Chambon P, Xu J (2004) Partially redundant functions of SRC-1 and TIF2 in postnatal survival and male reproduction. *Proc Natl Acad Sci USA* 101: 4453–4458

- Mendelson CR (2000) Role of transcription factors in fetal lung development and surfactant protein gene expression. *Annu Rev Physiol* 62: 875–915
- Mendelson CR (2009) Minireview: fetal-maternal hormonal signaling in pregnancy and labor. *Mol Endocrinol* 23: 947–954
- Mendelson CR, Montalbano AP, Gao L (2017) Fetal-to-maternal signaling in the timing of birth. *J Steroid Biochem Mol Biol* 170: 19–27
- Ming Z, Zou Z, Cai K, Xu Y, Chen X, Yi W, Luo J, Luo Z (2020) ARG1 functions as a tumor suppressor in breast cancer. *Acta Biochim Biophys Sin (Shanghai)* 52: 1257–1264
- Neri I, Monari F, Sgarbi L, Berardi A, Masellis G, Facchinetti F (2010) L-arginine supplementation in women with chronic hypertension: impact on blood pressure and maternal and neonatal complications. *J Matern Fetal Neonatal Med* 23: 1456–1460
- Neu J (2009) Effects of oral L-arginine on the pulsatility indices of umbilical artery and middle cerebral artery in preterm labor. *Yearbook of Neonatal and Perinatal Medicine* 2009: 63–64
- Nikolic MZ, Sun D, Rawlins EL (2018) Human lung development: recent progress and new challenges. *Development* 145: dev163485
- Norman JE, Shennan AH (2013) Prevention of preterm birth—why can't we do any better? *Lancet* 381: 184–185
- Okun JG, Conway S, Schmidt KV, Schumacher J, Wang X, de Guia R, Zota A, Klement J, Seibert O, Peters A et al (2015) Molecular regulation of urea cycle function by the liver glucocorticoid receptor. *Mol Metab* 4: 732–740
- Petraglia F, Imperatore A, Challis JR (2010) Neuroendocrine mechanisms in pregnancy and parturition. *Endocr Rev* 31: 783–816
- Phuc Le P, Friedman JR, Schug J, Brestelli JE, Parker JB, Bochkis IM, Kaestner KH (2005) Glucocorticoid receptor-dependent gene regulatory networks. *PLoS Genet* 1: e16
- Rizzo A, Trisolini C, Spedicato M, Mutinati M, Minoia G, Sciorsci RL (2011) *In vitro* effects of L-arginine on spontaneous and homocysteine-induced contractility of pregnant canine uteri. *Theriogenology* 76: 715–720
- Romero R, Dey SK, Fisher SJ (2014) Preterm labor: one syndrome, many causes. *Science* 345: 760–765
- Simmons LE, Rubens CE, Darmstadt GL, Gravett MG (2010) Preventing preterm birth and neonatal mortality: exploring the epidemiology, causes, and interventions. *Semin Perinatol* 34: 408–415
- Sin YY, Baron G, Schulze A, Funk CD (2015) Arginase-1 deficiency. *J Mol Med (Berl)* 93: 1287–1296
- Singh M, Padhy G, Vats P, Bhargava K, Sethy NK (2014) Hypobaric hypoxia induced arginase expression limits nitric oxide availability and signaling in rodent heart. *Biochim Biophys Acta* 1840: 1817–1824
- Sivashanmugam M, J J, V U, K N S (2017) Ornithine and its role in metabolic diseases: an appraisal. *Biomed Pharmacother* 86: 185–194
- Song P, Theodoratou E, Li X, Liu L, Chu Y, Black RE, Campbell H, Rudan I, Chan KY (2016) Causes of death in children younger than five years in China in 2015: an updated analysis. *J Glob Health* 6: 020802
- Stashi E, York B, O'Malley BW (2014) Steroid receptor coactivators: servants and masters for control of systems metabolism. *Trends Endocrinol Metab* 25: 337–347
- Surate Solaligue DE, Rodríguez-Castillo JA, Ahlbrecht K, Morty RE (2017) Recent advances in our understanding of the mechanisms of late lung development and bronchopulmonary dysplasia. *Am J Physiol Lung Cell Mol Physiol* 313: L1101–L1153
- Sutton EF, Gemmel M, Powers RW (2020) Nitric oxide signaling in pregnancy and preeclampsia. *Nitric Oxide* 95: 55–62
- Szwarc MM, Lydon JP, O'Malley BW (2015) Steroid receptor coactivators as therapeutic targets in the female reproductive system. *J Steroid Biochem Mol Biol* 154: 32–38
- Tetel MJ, Acharya KD (2013) Nuclear receptor coactivators: regulators of steroid action in brain and behaviour. *J Neuroendocrinol* 25: 1209–1218
- Tiboni GM, Giampietro F (2000) Inhibition of nitric oxide synthesis causes preterm delivery in the mouse. *Hum Reprod* 15: 1838–1842
- Vadillo-Ortega F, Perichart-Perera O, Espino S, Avila-Vergara MA, Ibarra I, Ahued R, Godines M, Parry S, Macones G, Strauss JF (2011) Effect of supplementation during pregnancy with L-arginine and antioxidant vitamins in medical food on pre-eclampsia in high risk population: randomised controlled trial. *BMJ* 342: d2901
- Wang X, Burghardt RC, Romero JJ, Hansen TR, Wu G, Bazer FW (2015) Functional roles of arginine during the peri-implantation period of pregnancy. III. Arginine stimulates proliferation and interferon tau production by ovine trophectoderm cells via nitric oxide and polyamine-TSC2-MTOR signaling pathways. *Biol Reprod* 92: 75
- Weckman AM, McDonald CR, Baxter JB, Fawzi WW, Conroy AL, Kain KC (2019) Perspective: L-arginine and L-citrulline supplementation in pregnancy: a potential strategy to improve birth outcomes in low-resource settings. *Adv Nutr* 10: 765–777
- Winer N, Branger B, Azria E, Tsatsaris V, Philippe HJ, Roze JC, Descamps P, Boog G, Cynober L, Darmaun D (2009) L-arginine treatment for severe vascular fetal intrauterine growth restriction: a randomized double-blind controlled trial. *Clin Nutr* 28: 243–248
- Wu G, Morris SM (1998) Arginine metabolism: nitric oxide and beyond. *Biochem J* 336: 1–17
- Wu G, Imhoff-Kunsch B, Girard AW (2012) Biological mechanisms for nutritional regulation of maternal health and fetal development. *Paediatr Perinat Epidemiol* 26: 4–26
- Wu G, Bazer FW, Satterfield MC, Li X, Wang X, Johnson GA, Burghardt RC, Dai Z, Wang J, Wu Z (2013) Impacts of arginine nutrition on embryonic and fetal development in mammals. *Amino Acids* 45: 241–256
- Yallampalli C, Izumi H, Byam-Smith M, Garfield RE (1994) An L-arginine-nitric oxide-cyclic guanosine monophosphate system exists in the uterus and inhibits contractility during pregnancy. *Am J Obstet Gynecol* 170: 175–185
- You J, Chen W, Chen J, Zheng Q, Dong J, Zhu Y (2018) The oncogenic role of ARG1 in progression and metastasis of hepatocellular carcinoma. *Biomed Res Int* 2018: 2109865
- You S, Cui AM, Hashmi SF, Zhang X, Deng R (2020) Dysregulation of bile acids increases the risk for preterm birth in pregnant women. *Nat Commun* 11: 2111